

Assessing the Role of Compaction in the Formation of Adcumulates: a Microstructural Perspective

M. B. Holness^{1*}, Z. Vukmanovic¹ and E. Mariani²

¹Department of Earth Sciences, University of Cambridge, Downing Street, Cambridge CB2 3EQ, UK; ²Department of Earth, Ocean and Ecological Sciences, University of Liverpool, Jane Herdman Building, 4 Brownlow Street, Liverpool L69 3GP, UK

*Corresponding author. E-mail: marian@esc.cam.ac.uk

Received March 22, 2017; Accepted June 6, 2017

ABSTRACT

The formation of adcumulates necessitates the continued growth of primocrysts down to low porosities. Gravitationally driven viscous compaction at the base of a crystal mushy layer on the magma chamber floor, driven by the weight of the mushy layer itself, is commonly suggested as a significant process acting to drive out interstitial liquid and promote adcumulate formation. Compaction necessitates viscous deformation, by either dislocation creep or diffusion-controlled processes such as pressure-solution: many studies suggest that the foliations preserved in cumulates are a consequence of recrystallization during compaction, completely overprinting primary magmatic fabrics. We test the compaction hypothesis by looking for microstructural evidence of viscous deformation. A detailed examination of cumulates from the Skaergaard intrusion, East Greenland, demonstrates only limited crystal plastic deformation, with no correlation between the extent of dislocation creep and the calculated volume fraction of trapped liquid left in the cumulates. Although the evidence for diffusion-controlled deformation is often cryptic, there is an anti-correlation between apparent aspect ratio of plagioclase and the extent of adcumulate crystallization, contradicting previous hypotheses involving transposition of original magmatic fabrics by dissolution–reprecipitation. This is supported by the spatial distribution of compositional zoning in plagioclase, which demonstrates that pressure-solution or related diffusion-controlled processes were insufficient to obscure primary magmatic fabrics. The Skaergaard adcumulates did not form by viscous compaction. Instead we suggest that they formed by primary processes involving mass transport in a thin mushy layer. Compaction is most likely to occur in slowly cooled intrusions in which the bulk magma crystallizes abundant dense minerals. We present preliminary observations of microstructures in norites from the lower Main Zone of the Bushveld Intrusion, South Africa, and in plagioclase-rich cumulates from the Fe–Ti oxide-rich Baima Intrusion, SW China. The evidence for dislocation creep in both intrusions is unambiguous, although deformation was insufficient to obliterate all traces of the primary magmatic fabrics and unlikely to have been sufficient to significantly reduce the volume of interstitial liquid.

Key words: adcumulate; compaction; layered intrusion; Skaergaard

INTRODUCTION

Fractionation of silicate magmas necessitates the separation of residual liquid and solids. Because crystallization results in the formation of crystal-rich zones, or mushes, an important process driving fractionation is

the expulsion of the interstitial liquid from the mush. The mechanisms by which such expulsion occurs are not fully understood but are important, not only in mafic systems, but also for our understanding of the behaviour of the large crystal-rich bodies that are thought to

underlie continental silicic volcanic complexes (Cashman *et al.*, 2017). In this contribution, we address the problem by focusing on a question of particular relevance to mafic systems, that of the formation of adcumulates. Adcumulates are rocks formed almost exclusively of mineral grains that crystallized from the bulk magma (known as primocrysts), containing only minor quantities of material that crystallized from an evolved interstitial liquid (Wager *et al.*, 1960). Despite many decades of work, and its fundamental importance in our understanding of crystal mushes, the formation of adcumulates remains one of the outstanding problems of igneous petrology.

Suggested processes resulting in adcumulate formation fall into two broad groups. The first comprises mechanisms that result in primocryst growth during efficient chemical communication with the overlying bulk magma. Wager *et al.* (1960) suggested that adcumulate growth is a primary crystallization feature created by effective mass transport through the mush by diffusion, which may be facilitated by slow crystal accumulation and the effective removal of the latent heat of crystallization by convective currents in the bulk magma (Wager, 1963; Wager & Brown, 1968). Other researchers have suggested that adcumulates form when there is an optimum balance between *in situ* nucleation and crystal growth at the interface between the mush and the bulk magma (Campbell, 1978; Morse, 1986), perhaps enhanced by textural equilibration (Campbell, 1987). The final suggestion in this group is that adcumulates result from the uninterrupted growth of primocrysts as the interstitial liquid is continually replenished during compositional convection in the mush (Sparks *et al.*, 1985; Tait & Jaupart, 1992).

The second group of models is perhaps of more general relevance to igneous systems across the compositional range and is predicated on the expulsion of evolved interstitial melt from the mush. Bédard (2015) suggested that melt can be expelled from mush undergoing penetrative shearing: this mechanism is potentially of particular relevance to gabbros at mid-ocean ridges. Others have suggested that interstitial liquid is expelled via gravitationally driven compaction facilitated by crystal plastic deformation (Wager *et al.*, 1960; Irvine, 1980; Sparks *et al.*, 1985; Shirley, 1986; Tharp *et al.*, 1998; Meurer & Meurer, 2006; Tegner *et al.*, 2009; McKenzie, 2011; Schmidt *et al.*, 2012).

There is currently no consensus as to which of these various mechanisms predominates, or in which particular environments each mechanism may play an important role. The main reason for this lacuna in our understanding is that we do not yet have an agreed set of criteria by which we can distinguish between the record left by the various processes in fully solidified cumulates. The situation is unchanged since Sparks *et al.* (1985) stated: 'For the case of feldspathic adcumulate in slowly cooled intrusions diagnostic criteria to distinguish extreme surface adcumulus growth from extreme compaction have not been developed. Distinguishing

the two models from textural or geological evidence is important and presents an interesting challenge to petrologists.' The current contribution is an attempt to rectify this, at least in part, by arguing that the necessary diagnostic criteria can be provided by a critical and informed quantitative assessment of cumulate microstructure.

In this contribution, we focus on the hypothesis that interstitial liquid can be expelled by compaction. We first review what is known about magmatic fabrics and how they might be modified during deformation associated with compaction. A comparison of the predicted microstructural record with layered intrusions, with particular focus on the Skaergaard intrusion of East Greenland, is then used to assess the extent to which compaction plays a role in generating adcumulates. Although the scope of this contribution is limited to a detailed study of mafic rocks, we anticipate that our arguments and approach are equally applicable to silicic systems.

DEFINITIONS

The scope of this contribution covers several different fields within Earth and materials science. Because scientific terms may be used to mean different things by each scientific community, for clarity we define here our use of the terminology that is critical to understanding the main concepts discussed in this paper.

Fabric

We follow the usage of Vernon (2004), who defined a fabric as a descriptor of the shape and arrangement of the mineral grains and their spatial orientation. The term therefore encompasses preferred orientations of either crystal lattices (crystal preferred orientation, or CPO) or grain shapes (shape preferred orientation, or SPO), as well as microstructures characterized by the absence of preferred orientations.

Recrystallization

This involves the formation of new grains through the generation and migration of high-angle (10–15° misorientation) grain boundaries (Doherty *et al.*, 1997, and references therein). Although the formation of high-angle boundaries through progressive rotation of sub-grain boundaries is a process governed by recovery mechanisms, in Earth sciences this is referred to as sub-grain rotation recrystallization (Stipp *et al.*, 2002). Recrystallization is driven by stored deformation energy. When recrystallization occurs during deformation it is referred to as dynamic recrystallization.

Recovery

This process releases the strain energy stored in the system by the reorganization of dislocations to a lower energy configuration, forming sub-grain walls or sub-grain (low angle, <10°) boundaries. Recovery does not

require the migration of high-angle grain boundaries (Doherty *et al.*, 1997, and references therein).

Pressure solution (or dissolution–reprecipitation)

This is the process whereby rock deforms via the diffusion of matter along grain boundaries or through the volume of grains (Rutter, 1983). On a micro-physical level, this process is equivalent to diffusion creep, which is a grain-size sensitive process and is always accompanied by grain boundary sliding (e.g. McClay, 1977). However, for most geological usage, pressure solution (dissolution–reprecipitation) is assumed to involve deformation in the presence of a fluid phase and the rate of diffusion is dependent on the length of the diffusion pathways.

Viscous deformation

In this contribution, the term viscous deformation is used to refer to the flow of rocks that may deform by either dislocation creep (which is always accompanied by dynamic recrystallization), or by diffusive processes such as diffusion creep (which is always accompanied by grain boundary sliding) or pressure solution (in the presence of a fluid phase).

COMPACTION AS AN ADCUMULATE-FORMING PROCESS

Previous work

Compaction is envisaged as a process driven by an imbalance between the lithostatic and hydrostatic pressure in a porous layer in which the interstitial liquid has a lower density than the solids, and where the upwards flow of liquid is accompanied by viscous deformation of the solid crystal framework. Because the term compaction is also used to describe the overall reduction in volume of a crystal mush by the mechanical rearrangement of essentially rigid particles, in the present contribution we make a clear distinction between mechanical compaction and the more general use that implies viscous deformation.

The theoretical treatment of viscous compaction, primarily aimed at understanding the extraction of partial melt from the mantle, is set out in a series of papers (McKenzie, 1984, 1985; Richter & McKenzie, 1984; Scott & Stevenson, 1984, 1986; Fowler, 1990a, 1990b). The importance of understanding the migration of basic melts in the mantle led to a major effort to constrain the rheology of melt-bearing olivine-dominated systems (e.g. Cooper & Kohlstedt, 1986; Holtzman *et al.*, 2003; King *et al.*, 2009). The more complex of the theoretical treatments of compaction include consideration of specific deformation mechanisms likely to operate in the mantle, such as simultaneous grain boundary diffusion creep and power law creep (Tharp *et al.*, 1998) or granular flow (Rutter, 1997).

The concept that adcumulates in crustal magma chambers might form by compaction was first explored

by Irvine (1980), who observed that the boundaries between major cyclic units in the Muskox intrusion, defined by changes in modal mineralogy, do not coincide with discontinuities in the chemical composition of minerals. He argued that this was caused by upward flow of differentiated intercumulus melt in response to gravitationally driven compaction of the cumulate pile.

A theoretical compaction model was first applied to layered intrusions by Sparks *et al.* (1985), who used experimental work on mantle compositions to make assumptions about the rheology of an olivine-dominated crystal mush. The rheology and deformation mechanisms that might operate in a gabbroic, plagioclase- and pyroxene-dominated, crystal mush undergoing compaction are not well constrained, although if one assumes that compaction did happen the bulk viscosity of the crystal mush can be deduced by fitting a theoretical compaction model to the observed spatial variation of bulk-rock composition (e.g. Tegner *et al.*, 2009; McKenzie, 2011). The required value of the bulk viscosity can then be used to infer the mechanisms by which the crystal framework deforms (McKenzie, 2011). Importantly, however, it can only be proved that compaction is indeed a significant process in layered intrusions if the microstructures preserved in adcumulates are consistent with viscous deformation during compression. No previously published study advocating compaction as a significant process in layered mafic intrusions involves a detailed, comprehensive and critical analysis of microstructures preserved in adcumulates, and therefore no conclusive supporting evidence is provided that adcumulates actually resulted from compaction.

What do cumulate microstructures record?

Before we can answer the question of whether or not compaction is a significant process in the creation of adcumulates, there are further, more fundamental questions that must be answered: to what extent are cumulate microstructures and fabrics primary magmatic features and how much have they been modified post-accumulation?

Wager & Deer (1939) coined the term ‘igneous lamination’ in acknowledgement of their belief that foliations and lineations (defined by an SPO of non-equant grains) in the Skaergaard cumulates were created at the interface between the mush and the bulk magma by prismatic alignment in response to the action of currents: they therefore preserve some record of processes active at, or close to, the top of the crystal mush. The literature contains a large number of studies based on this *a priori* assumption, using fabrics to develop models of mass-transport processes occurring in the magma chamber (e.g. Brothers, 1964; Wager & Brown, 1968; Irvine & Stoesser, 1978; Irvine, 1983; Shelley, 1985, 1986; O’Driscoll *et al.*, 2007, 2008). However, there is a smaller, but still significant, number of studies that

spring from an equally *a priori* assumption that foliations and lineations preserved in layered intrusions result from the complete obliteration of the original magmatic microstructure by post-accumulation, compaction-driven, recrystallization during viscous deformation (e.g. Boudreau & McBirney, 1997; McBirney & Nicolas, 1997; Meurer & Boudreau, 1998; Boorman *et al.*, 2004). In many cases the fabrics discussed by the two groups are indistinguishable.

Interestingly, this dichotomy only really exists in the body of published work concerning layered mafic intrusions in the continental crust. The indisputable near-ubiquity of viscous deformation, either syn-magmatic or just under the solidus, at mid-ocean ridges, means that there is a consensus in the literature on oceanic gabbros concerning the distinction between primary, unrecrystallized, igneous microstructures and those that have been recrystallized during viscous deformation (e.g. Satsukawa *et al.*, 2013).

The foliated olivine cumulates of the Rum Layered Intrusion, in which the olivine mode reaches 95 vol. % (e.g. Worrell, 2002) with a corresponding liquid fraction of only a few vol. %, provide a good example of the dichotomy of interpretation and a pointer towards its resolution. Whereas Brown (1956) and Wager & Brown (1968) argued that the formation of such extreme accumulates necessitates a slowly accumulating (essentially undeforming) mush through which diffusion is sufficiently effective that primocrysts in the mush can continue to grow with the same composition, Sparks *et al.* (1985) used them as an illustrative example for calculations of the time- and length-scales of compaction (with the underlying, but unstated, assumption that they have undergone viscous deformation). However, a detailed study of the olivine cumulates of the Ard Mheall Member of the Rum Western Layered Series, using quantitative microstructural analysis, geochemistry and electron backscatter diffraction (EBSD), revealed no evidence of deformation or crystal draping that could be used in support of viscous compaction (Worrell, 2002). Instead, Worrell concluded that the foliation was created by settling of non-equant grains, followed by mechanical rearrangement and overgrowth of the olivine grains during compositional convection. Closely related olivine cumulates, containing up to 85 vol. % olivine, occur in pipe-like structures outside the main layered complex of Rum. Holness *et al.* (2012b) argued, using EBSD data combined with an analysis of the spatial arrangement of the olivine grains and the absence of evidence of significant plastic deformation that, in agreement with Worrell (2002), post-accumulation microstructural modification in these pipes was limited to the mechanical rearrangement and overgrowth of essentially rigid grains. The resolution of the significance of viscous compaction, and the extent of the crystal plastic deformation mechanisms that may accompany it, therefore lies in a detailed and critical analysis of microstructures, fabrics and fabric formation in layered intrusions (e.g. Hunter, 1996).

MICROSTRUCTURES AND FABRIC FORMATION IN LAYERED INTRUSIONS

The development of microstructures and fabrics in layered intrusions occurs between the liquidus and the solidus, but may extend into the subsolidus. Subsolidus microstructural evolution driven, for example, by post-solidification deformation and annealing, is not pertinent to the question of how accumulates form but may obscure the record of processes that are. In the following, we describe the magmatic processes and deformation mechanisms that might affect microstructure and create preferred grain orientations in cumulates, and we outline what diagnostic microstructural criteria might be used to distinguish between them. The different mechanisms are discussed in a sequence that reflects the timing of their significance relative to the solidification history of the mushy layer.

Primary fabric formation during accumulation

Fabrics defined by a shape preferred orientation (SPO) may form during settling of non-equant grains from either a static or a moving magma (e.g. settling from dense crystal-laden currents). SPOs may also form as flowing magma rearranges non-equant grains at the interface between the mush and the bulk magma (Grout, 1918). These fabrics form in the suspension flow regime (Nicolas, 1992), above what is variously termed the critical melt fraction (Arzi, 1978; van der Molen & Paterson, 1979), the rigid percolation threshold (Vigneresse & Tikoff, 1999), and the solid-to-liquid transition (Rosenberg & Handy, 2005); the melt fraction where this transition occurs is dependent on grain shape (Picard *et al.*, 2013). In this regime, termed granular flow by Rutter & Neumann (1995), crystals behave generally as rigid, isolated, objects (although some might form clusters) suspended in the flow, and the viscosity of the system is low. In a dense suspension, some grains may become plastically deformed, but only weakly so (Nicolas, 1992; McBirney & Nicolas, 1997).

Fabrics created by grain rearrangement by flowing magma are defined by both SPO and a crystallographic preferred orientation (CPO) of non-equant primocrysts, although the SPO may be modified by later overgrowth, leading to partial or complete obscuring of any original shape-defined fabric (Brothers, 1964). Interstitial minerals cement the progressively solidifying mush and have neither an SPO nor a CPO. SPO fabrics are either foliations or lineations, with the type and strength of the preferred orientation dependent on the particle shape, the concentration of particles and the extent to which they interact with each other, and the shear strength (Yamamoto & Matsuoka, 1996). Although the precise details of these relationships are not known for magmatic systems (in which particles may be cohesive), the sedimentary literature suggests that elongate clasts can be either aligned parallel to the shear direction (Rust, 1972; Davies & Walker, 1974; Yamamoto & Matsuoka,

1996), or aligned parallel to the vorticity axis and perpendicular to the flow direction (Rust, 1972; Iso *et al.*, 1996; Yamamoto & Matsuoka, 1996). Foliations, rather than lineations, are formed when the particle concentration is high (Yamamoto & Matsuoka, 1996), although a high particle concentration may also weaken the strength of any fabric, owing to particle interactions (Ildefonse, 1987; Iso *et al.*, 1996; Rust, 1972). Particles undergo tiling to form imbrications, thus preventing free rotation of individual particles (Rust, 1972; Mainprice & Nicolas, 1989), particularly if the particles have a high aspect ratio (Benn & Allard, 1989). Tiling cannot be created during solid-state deformation and so is an unambiguous indicator of fabrics formed at the interface between the mush and the bulk magma (Nicolas, 1992).

The common non-equant primocryst minerals in gabbros are plagioclase, olivine and pyroxene (with the addition of volumetrically minor apatite in more evolved cumulates). Because plagioclase most generally shows the greatest departure from an equant shape, and preferred orientations are best developed for the more non-equant minerals (e.g. Brothers, 1964), fabrics are dominated by a preferred plagioclase orientation. Unimpeded growth of plagioclase crystals generally creates tabular grains dominated by (010) faces, which may be elongated along either [001] (e.g. Kirkpatrick, 1974; Klein & Ullmann, 1974) or [100] (Gay & Muir, 1962; Nwe, 1975; Fenn, 1977; Swanson, 1977). Foliations formed by magmatic flow will therefore be formed by the alignment of plagioclase (010) planes, whereas [001] or [100] axes may define a lineation, which is generally interpreted to be parallel to the magma flow direction (e.g. Brothers, 1964; Nwe, 1975; Holness & Humphreys, 2003; Morales *et al.*, 2011; Satsukawa *et al.*, 2013; Hoyer & Watkeys, 2015).

Brown (1956, p. 16) described the packing of plagioclase crystals in troctolitic cumulates from Rum: 'Sections parallel to the lamination show the inter-grain boundaries between feldspars [sic] to be much more irregular than do sections perpendicular to this plane, where the grain boundary, subparallel to the crystallographic (010) plane, intersects the plane of section in almost a straight line. This suggests that the tablets were deposited with their (010) planes almost in contact, as now seen, and that interprecipitate growth was thereby restricted to directions perpendicular to *b*.' This type of selective modification of an original SPO, involving an increase of the original aspect ratio of the plagioclase tablets, and the retention of planar grain boundaries parallel to the (010) planes of both the grains involved, is highly supportive of the foliation being a primary magmatic fabric, formed by the alignment of tabular plagioclase grains at the interface between the mush and the bulk magma that places the (010) faces of adjacent grains in contact with each other.

Olivine tends to grow as flattened tablets parallel to (010), elongate along [001]. Any fabrics defined by a

primary SPO resulting from rearrangement in magmatic currents will therefore be dominated by foliations created by the alignment of (010), and lineations by the alignment of [001] (Benn & Allard, 1989).

Secondary fabric formation immediately following accumulation

The formation of secondary fabrics by the mechanical rearrangement of crystals occurs in the transition between suspension flow and solid state, in which liquid fractions are high but the crystals tend to form clusters or chains. This state approximates to the magmatic flow of Nicolas (1992) and occurs below the rigid percolation threshold of Vigneresse & Tikoff (1999). As they get caught up with others in the loose crystal framework, crystals may take up some plastic strain (Nicolas, 1992).

Paterson (1995, 2001) and Rutter (1997) argued, from a theoretical standpoint, that deformation in a melt-bearing system may occur by grain boundary sliding, with intergranular interferences accommodated by localized dissolution and reprecipitation, permitting the relative movement of essentially rigid grains even at very low porosities, particularly if a high proportion of grain boundaries contain melt films (Paterson, 2001). They called this process diffusion-assisted granular flow [although this is not the granular flow described by Rutter & Neumann (1995), which occurs at high melt fractions]. We would expect a diffusion-assisted deformation mechanism such as this to be active at low stresses. However, no unambiguous experimental or observational evidence has been published demonstrating that diffusion-assisted granular flow is significant in either synthetic or natural materials [although see Mecklenburgh *et al.* (2006), who presented circumstantial evidence that might suggest its operation].

Neither Paterson (1995, 2001) nor Rutter (1997) considered microstructure and the effect of diffusion-assisted granular flow on non-equant grains. By itself, mechanical rotation (i.e. with no grain boundary sliding) of rigid non-equant particles undergoing compression is not sufficient to create a strong SPO, even for a 50% reduction of porosity (Higgins, 1991; Nicolas, 1992), although there is a detectable change from an originally isotropic fabric to an anisotropic fabric. However, this weak SPO could be enhanced if the particles were free to slide past each other during granular flow. Locally there might be microstructural evidence of dissolution-precipitation (see the following section).

In contrast to Paterson (1995, 2001) and Rutter (1997), Philpotts *et al.* (1996) argued, from observation of ponded lava flows ~100 m thick, that gravitationally driven compaction achieved by the mechanical rearrangement of non-deforming grains can occur only in a narrow window between the formation of the crystal frameworks and the time when crystallization has proceeded sufficiently to strengthen the framework. From an analysis of bulk-rock compositions in the Holyoke

flood-basalt flow they suggested that this window is open only when the mush is ~ 33 vol. % solid. The draping of (undeformed) plagioclase crystals around larger grains of olivine in troctolitic cumulates (e.g. Hunter, 1996), and the common observation that plagioclase grains inside oikocrysts are commonly randomly oriented, whereas those outside drape around the oikocryst (e.g. Higgins, 1991), may be a consequence of mechanical compaction in this high-porosity regime.

A careful consideration of the anisotropy of plagioclase grain orientations in the 300 m thick Palisades sill revealed evidence for ~ 10 vol. % compaction owing to collapse of previously isotropic plagioclase frameworks (Gray *et al.*, 2003). This elegant result was developed by Philpotts & Philpotts (2005), who showed that the degree of anisotropy of plagioclase frameworks and chains in the 70 m thick Cohasset flow corresponds closely to the distribution of incompatible elements (and thus to the distribution of residual liquid during solidification). Mechanical compaction of 10–20 vol. % in the lower part of the flow was achieved by rearrangement of essentially rigid grains, with only minor plastic deformation of the larger phenocrysts, resulting in the upwards expulsion of liquid.

Secondary fabrics may also form in the upper, high-porosity, unconsolidated parts of the mush by shear caused by wholesale pre-consolidation slumping (e.g. Higgins, 1991; Meurer & Boudreau, 1998; O'Driscoll *et al.*, 2007, 2008; VanTongeren *et al.*, 2015) or during grain-supported flow during pluton-scale events (Paterson *et al.*, 1998). These processes will create a matching SPO and CPO recorded by non-equant prismatic crystals, although any SPO may be obscured by overgrowth. This mechanism is manifest at outcrop scale by soft-sediment structures such as slumped and contorted layering, formed by gravitational instabilities of an unconsolidated crystal pile on a sloping magma chamber floor (e.g. Emeleus *et al.*, 1996; O'Driscoll *et al.*, 2007).

Although the porosity of the slumping crystal mush is relatively low and crystals interact with each other during deformation, in slumped, plagioclase-dominated, cumulates of the Rum Eastern Layered Intrusion there is almost no evidence of viscous deformation by either dislocation creep (O'Driscoll *et al.*, 2007) or recrystallization (Tepley & Davidson, 2003). Slumped gabbros in the Fluxion Gabbros of the Ardnamurchan Centre 3 also show no evidence of viscous deformation (O'Driscoll *et al.*, 2008). None of these studies considered the possibility of accommodation of grain interference by localized dissolution–reprecipitation [as advocated by Paterson (1995, 2001)].

Fabrics formed by shear during slumping of gabbros are foliations defined by the preferred orientation of tabular plagioclase flattened on (010) (Brothers, 1964; O'Driscoll *et al.*, 2007). If the grains are elongate, this may be associated with a lineation, defined by an SPO and an associated CPO, parallel to the strike of the foliation (Brothers, 1964; Housden *et al.*, 1995; O'Driscoll

et al., 2007; VanTongeren *et al.*, 2015). In contrast, fabrics attributed to slumping in Ardnamurchan Centre 3 (O'Driscoll *et al.*, 2008) comprise a foliation defined by alignment of plagioclase (010) faces associated with an SPO lineation that is perpendicular to the strike of the foliation.

Tertiary fabrics and microstructures formed by recrystallization of low-porosity mush

The theoretical models of viscous compaction posit a driving force provided by the mass of overlying crystals: thus, compaction occurs at and near the base of the mush. Here the porosity is low, interstitial minerals have begun to crystallize and grain boundaries have begun to form between mineral grains. Deformation of the solid crystal framework can no longer occur by the mechanical rearrangement of essentially rigid grains, but instead proceeds by changing the shape of individual crystals by plastic strain or dissolution–reprecipitation (i.e. diffusive mass transfer by solution).

Microstructures and fabrics formed during dislocation creep

During dislocation creep a high free dislocation density forms in response to the stress experienced by the system. Lattice misorientations (shown by undulose extinction and low-angle boundaries) and (tapering) mechanical twins (Nicolas, 1992) are ubiquitous. Extensive plastic deformation by dislocation creep results in a CPO, controlled by the slip systems active during deformation, and an SPO that is required to accommodate the changes in volume during deformation. Dislocation creep is always accompanied by recrystallization, which annihilates dislocations or recovers them into sub-grains and grain boundaries while the continuing deformation continually generates new dislocations. The complete obliteration of an original fabric by plastic deformation, accompanied and/or followed by recrystallization, requires large strain and sustained high temperatures.

Plagioclase CPOs in high-grade foliated metamorphic rocks consist of the alignment of the (010) planes roughly parallel to the rock foliation, with either [100] or [001] subparallel to any lineation (Olesen, 1987; Mainprice & Nicolas, 1989). This is consistent with the experimental observation that the dominant slip system in plagioclase is (010)[001] (Olsen & Kohlstedt, 1984; Montardi & Mainprice, 1987; Ji *et al.*, 1988; Ji & Mainprice, 1990; Svahnberg & Piazzolo, 2010). In contrast, a more characteristic fabric in plastically deformed oceanic gabbros is a lineation defined by the preferred alignment of [100] (Satsukawa *et al.*, 2013). This is thought to occur when crystal-plastic deformation overprints, and is subparallel to, a pre-existing strong magmatic foliation—in such a case the grains are already favourably oriented to permit the activation of the (010)[100] slip system (Satsukawa *et al.*, 2013). A detailed study of plagioclase mylonites in oceanic

gabbros also found a similar fabric, with [100] parallel to the lineation and (010) oriented in the foliation (Mehl & Hirth, 2008), suggestive of slip on (010)[100], with some fabrics suggestive of the operation of the (001)[100] system.

In the case of olivine, fabrics caused by deformation-induced lattice rotation and recrystallization under simple shear are well documented, particularly in mantle peridotites. The dominant active slip system (and hence the resultant preferred orientation) depends on stress, temperature and H₂O content (Carter & AvéLallemant, 1970; Jung & Karato, 2001; Katayama *et al.*, 2004). Four main fabrics are observed: A-type fabrics are characterized by the (010) plane parallel to the shear plane, with the [100] direction parallel to the shear direction: they are formed by slip on (010)[100] and are characteristic of dry systems at low temperatures under a wide range of stress. B-type fabrics are characterized by the (010) plane parallel to the shear plane, with the [001] axis parallel to the shear direction: they are formed by slip on (010)[001] and are characteristic of moderate H₂O contents, a wide temperature range and high stress. C-type fabrics are characterized by the [001] axis parallel to the shear direction and the (100) plane parallel to the shear plane; they are formed by slip on the (100)[001] system and are dominant at high temperatures, high H₂O contents and mid to low stress. E-type fabrics are created by slip on (001)[100] at moderate temperatures and H₂O contents and high strain, and are characterized by the (001) plane parallel to the shear plane and [100] parallel to the shear direction. It is not clear which of these slip systems would dominate under the conditions experienced in layered intrusions, but it is likely to be the A-type system.

At low temperature and/or high strain, the dominant slip system for clinopyroxene is (100)[001] (AvéLallemant, 1978; Ashworth, 1980, 1985), whereas at high temperature and/or low strain multiple slip systems can operate ((110)_{1/2} [110], (110)[001], (100)[001] and (010)[100]) (Van Roermund & Boland, 1981; Van Roermund, 1984; Bautier *et al.*, 1991; Ingrin *et al.*, 1991; Philippot & van Roermund, 1992). We would therefore expect a wide range of possible fabrics to result from dislocation creep.

Recrystallization driven by static annealing of rocks deformed by dislocation creep

If the rock is cooled immediately after deformation, preventing static recrystallization, then both CPOs and SPOs created during dislocation creep will be preserved. However, if the temperature remains high (>500°C for plagioclase) after the cessation of deformation, recrystallization will continue under static conditions if the dislocation density in the crystals is sufficiently high. The final microstructure in this case is likely to retain some record of the CPO formed during deformation, but any SPO will be lost. In particular, all evidence will be erased of low-index faces created while

primocrysts were growing in contact with abundant liquid. The microstructure will become granular [i.e. it will reach textural equilibrium (Hunter, 1996)]. If the temperature remains high after the microstructure has closely approached textural equilibrium then normal grain growth will start (driven by the reduction in interfacial energy and characterized by the migration of grain boundaries towards their centre of curvature), resulting in a coarse-grained granular microstructure with no SPO but with an inherited CPO. In general, evidence for static recrystallization, textural equilibration and normal grain growth of fully solidified cumulates in coarse-grained polymineralic plutons in the shallow crust is localized, confined to chill zones and monomineralic regions of polymineralic rocks (e.g. Hunter, 1996; Holness *et al.*, 2012a). Static recrystallization is therefore likely to increase in significance as the size and depth of intrusion increases.

Fabric development by dissolution–reprecipitation

At low stresses, viscous deformation occurs by diffusive processes. Although the layered intrusion community commonly refers to a process of dissolution–reprecipitation (e.g. Meurer & Boudreau, 1998), this is essentially pressure-solution, driven by stress-induced chemical potential gradients (Rutter, 1983). It is also closely related to diffusion creep, which is associated with grain boundary sliding, and the hypothesized diffusion-assisted granular flow of Paterson (2001) at low porosities.

Boorman *et al.* (2004) found a relationship between strength of foliation (defined by an SPO), aspect ratio and the amount of interstitial liquid, together with the absence of a lineation, in orthopyroxenites from the Bushveld Intrusion. They suggested that unfavourably oriented grains acquire a high dislocation density during viscous compaction and so dissolve. The mechanism they invoked is therefore a combination of plastic strain and recovery via dissolution–reprecipitation, with the implicit assumption that the recrystallization process ran to completion, as they presented no evidence of the incomplete recrystallization that is so common in regional metamorphic terranes.

A recent experimental study by Schmidt *et al.* (2012) was focused on the settling and compaction of an accumulation of olivine crystals in basaltic melt undergoing centrifugation. They found that the porosity in the settled crystal accumulation reduced from a starting point of 54 vol. % to ~30 vol. %. This final porosity is greater than can be achieved by ordered close packing of spheres (26 vol. %) but less than that expected for monodisperse random close packing (36.6 vol. %; Song *et al.*, 2008). Schmidt *et al.* (2012) argued that the process whereby the porosity was reduced during centrifugation is dissolution–reprecipitation [but it is possible that the microstructures they observed are a consequence of grain boundary formation during sintering

(e.g. German *et al.*, 2009), driven by the reduction of interfacial energies as grains come into contact with each other].

Importantly, viscous deformation by a diffusion mechanism will not always be easy to identify. Typical signatures of diffusion-controlled deformation are the truncation of grains of a known original shape, together with interpenetration of grains and the development of sutured contacts, and compositionally distinct overgrowths on faces oriented so that they are under relatively low stress (McClay, 1977; Rutter, 1983; Cooper & Hunter, 1995). However, apparently sutured grain boundaries can be created during primary solidification in the absence of deformation (Holness *et al.*, 2007). Furthermore, highly irregular grain boundaries created during diffusion-controlled deformation are likely to become smooth during cooling, particularly between two grains of the same phase, driven by the reduction of interfacial energies (Hunter, 1996).

Although the absence of CPO is generally used as evidence that deformation occurred primarily by dissolution/precipitation creep (Karato, 1988; Rutter *et al.*, 1994), Miyazaki *et al.* (2013) demonstrated that a CPO can occur during deformation dominated by diffusive processes: in melt-bearing olivine aggregates formed of euhedral grains, grain boundary sliding occurs preferentially on boundaries formed of specific crystallographic planes, leading to grain rotation and a CPO (and an associated SPO).

Meurer & Boudreau (1998) also argued that fabrics defined by a CPO and associated SPO in anorthosites and troctolites from the Stillwater Intrusion formed by a dissolution–reprecipitation process. They reported a strong correlation between the strength of foliation and the plagioclase average apparent aspect ratio and suggested that the fabrics were created under uniaxial stress (gravitationally driven compaction) by the selective resorption of unfavourably oriented grains and uneven growth of crystals. This hypothesis is based on the (implicit) assumption that resorption/dissolution is fastest in directions parallel to (010). However, for hydrous systems the fastest dissolution of plagioclase occurs normal to (010) and the slowest dissolution direction is normal to the (001) plane (Arvidson *et al.*, 2004). Such anisotropy of dissolution and grain growth will indeed lead to the creation of a CPO, characterized by the crystallographic direction with slow dissolution and growth rates facing the maximum shortening direction, whereas directions with fast rates face the maximum extension direction (Bons & den Brok, 2000). Dissolution–reprecipitation of plagioclase (at least in a system containing hydrous fluid) will therefore create a CPO fabric with the [100] axes predominantly perpendicular to the compression direction whereas the (010) faces and poles to (001) are aligned parallel to the compression direction (Heidelbach *et al.*, 2000; Arvidson *et al.*, 2004). Grains will be elongated in a direction perpendicular to the (010) faces (Svahnberg & Piazzolo, 2013), instead of parallel to (010) as described by Meurer & Boudreau (1998).

The effect of deformation on primary magmatic compositional zoning

Importantly, deformation by either dislocation creep or diffusive processes such as dissolution–reprecipitation or diffusion creep results in the partial or complete replacement of compositional zoning formed during the early stages of crystallization. Magmatic zoning is typically parallel to growth faces (dominantly low-index faces; Fig. 1a), and strongly zoned mineral grains may contain a core recording their original shape. This provides the opportunity to identify any grain interpenetration by pressure-solution. More generally, dissolution–reprecipitation will obliterate all grain boundaries defined by growth faces on primocrysts and create discontinuities in the magmatic compositional zoning, associated with a localized loss of planar growth faces, particularly at high-pressure points created where grains impinge at a high angle. For the particular case of plagioclase, Svahnberg & Piazzolo (2013) showed that the anisotropy of dissolution–reprecipitation results in zoning with the thickest rims on the (010) faces of grains oriented with the (001) faces subparallel to foliation (Fig. 1b). Thus, compositional zoning resulting from dissolution–reprecipitation will not necessarily have any relationship with low-index crystallographic planes associated with primary growth at or near the interface between the mush and the bulk magma, but will be oriented relative to the maximum principal stresses that are causing dissolution.

Any primary magmatic zoning is likely to be obliterated during the recrystallization that accompanies dislocation creep: neoblasts on grain boundaries are likely to be unzoned, and migrating grain boundaries will create grain margins with a composition inherited from the adjacent replaced grain. Recrystallization may sometimes result in the creation of new grains with a different composition from that of the original stressed grains, but in most cases this difference reflects the fact that the recrystallization occurred at a different temperature than that for the growth of the original grains (Tullis, 1975).

A NATURAL LABORATORY: THE SKAERGAARD INTRUSION

The Skaergaard intrusion has been the touchstone for studies of layered intrusions since Wager & Deer (1939) set out their vision of a closed, essentially sedimentary, system undergoing progressive fractionation. The Skaergaard archive, particularly those studies published in 1997 and 1998, perfectly illustrates the dichotomy between researchers who interpret the preserved microstructures as a record of processes occurring at, or close to, the interface between the mush and the bulk magma and those who argue that little remains of the original microstructure and that the cumulates have undergone extensive recrystallization during viscous compaction. The Skaergaard intrusion thus presents an excellent opportunity to test the competing ideas about

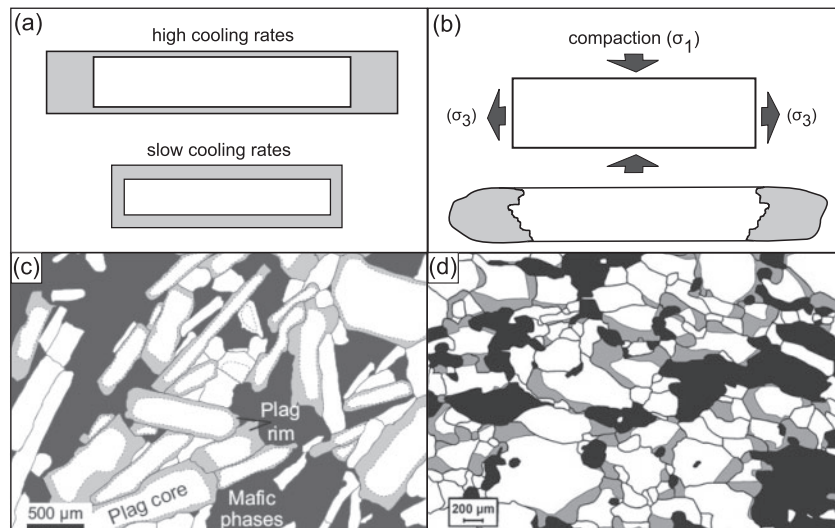


Fig. 1. Schematic representations of zonation in plagioclase. (a) Concentric zones develop parallel to low-index growth faces when plagioclase is grown from a magma, with a core formed when the crystal was in contact with abundant liquid and the zoned margins formed from growth during *in situ* fractionation in the crystal mush. (b) Zoning formed during dissolution–reprecipitation creates zones oriented relative to the compressive stress. (c) Schematic illustration showing growth zoning in an unmodified igneous cumulate. (d) Asymmetric zoning formed during viscous deformation by dissolution–reprecipitation, reproduced from Svahnberg & Piazzolo (2013) with permission from Springer.

adcumulate formation and the origin of fabrics preserved in cumulates.

Geological setting

The Skaergaard intrusion formed from the injection of a large (8 km × 11 km × 4 km; Nielsen, 2004) body of tholeiitic basalt into a fault-bounded space (Irvine *et al.*, 1998) on the extending margin of East Greenland during the opening of the North Atlantic. The intrusion lies at the unconformity between Precambrian gneisses and an overlying sequence of Eocene plateau lavas (Wager & Deer, 1939) to which the Skaergaard magma is closely related (Nielsen, 2004; Jakobsen *et al.*, 2010) (Fig. 2). Once the chamber inflated to its final size (Holness *et al.*, 2007, 2015) it remained closed both to further magma replenishment and to eruption, crystallizing to form one of the world's best examples of extreme fractionation of a basaltic magma.

Solidification resulted in the formation of three series, first defined by Wager & Deer (1939): the (volumetrically dominant) Layered Series crystallized upwards from the floor; the Marginal Border Series (MBS) crystallized inwards from the (vertical) walls; the Upper Border Series (UBS) crystallized downwards from the roof (Fig. 2). The Layered Series and Upper Border Series meet at the Sandwich Horizon. The Layered Series is divided into Lower, Middle and Upper Zones based on the absence of cumulus olivine in the Middle Zone. The Lower Zone is subdivided into LZa (containing cumulus olivine and plagioclase), LZb (with cumulus augite) and LZc (with cumulus Fe–Ti oxides). The Hidden Zone (HZ) is the unexposed material underlying LZa; it is sampled by a single drill core [the Cambridge drill core, described by Holness *et al.* (2015), location

shown in Fig. 2]. The Upper Zone is also subdivided; the base of UZb defines the arrival of cumulus apatite, whereas the base of UZc marks the first appearance of the mosaic form of ferro-hedenbergite inverted from β -ferrobustamite. The UBS [Salmonsens & Tegner, 2013; although see Naslund (1984)] and MBS (Hoover, 1989) can be similarly subdivided.

Building on the earlier work of McBirney (1975), recent studies have highlighted the importance of liquid immiscibility during solidification, and particularly the preferential loss of an immiscible Si-rich conjugate from the interstitial liquid in the floor cumulates through much of the stratigraphy between LZc and UZa (Holness *et al.*, 2011), creating a dense Fe-rich interstitial liquid. Such preferential loss of liquid from the floor mush would leave an unrepresentatively Fe-rich bulk composition in the fully solidified floor sequence (Nielsen *et al.*, 2015). At the higher levels in the stratigraphy, the coexistence of grain-scale pockets of granophyre and patches of ilmenite intergrown with a variety of minerals marks the point above which silica-rich conjugate liquid (now solidified to granophyre) was no longer lost to the overlying bulk magma but was retained in the mush (Holness *et al.*, 2011).

The western outcrop of the upper part of UZa is notable for a series of gently plunging synformal structures known as trough bands (Wager & Deer, 1939)—these features are 10–50 m wide, with an axial plane approximately perpendicular to the chamber walls (the location and axial trends of which are shown in Fig. 2), and are separated by elongate reef-like mounds of massive ferrogabbro (Irvine, 1983). The trough bands are defined by modal layering with a melanocratic base grading steeply upwards into plagioclase-rich material (Fig. 3). These graded layers are typically (Fig. 3a) (but not

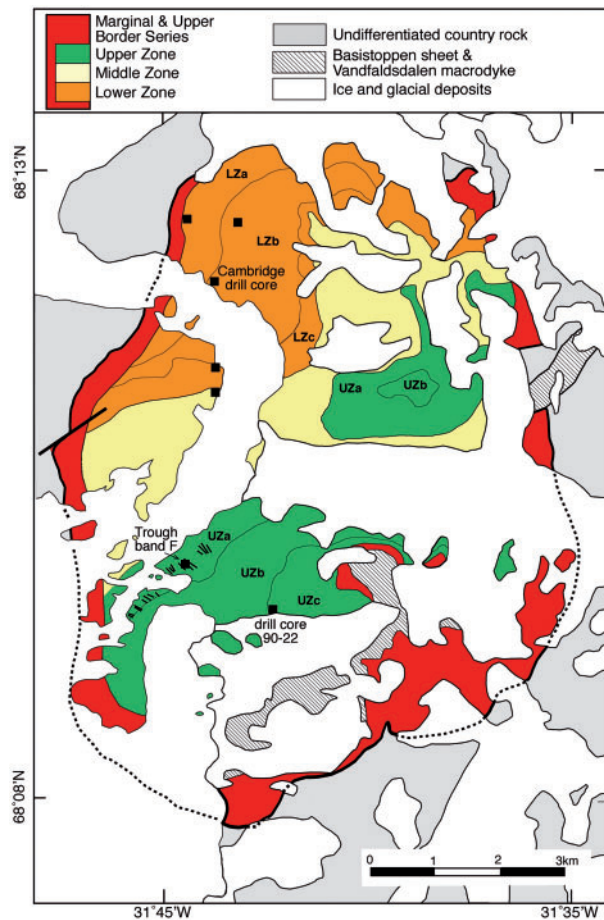


Fig. 2. Simplified geological map of the Skaergaard intrusion, after [McBirney \(1989b\)](#). The locations of the samples studied here are shown as black squares, with the position of the two drill cores also shown. The trough bands are shown schematically as lines parallel to the trough axis.

always; [Fig. 3b](#) and [c](#)) separated by variable thickness of homogeneous gabbro, and are thickest at the trough axis. Some trough bands can be traced for ~ 300 m along their axis and for more than 100 m stratigraphically ([Irvine & Stoesser, 1978](#)). Although some are relatively shallow ([Fig. 3a](#)), the steepest (outer) parts of the limbs of some of the trough bands are locally inclined some 100° from each other ([Fig. 3b](#); [Wager & Brown, 1968](#)). When rotated back to the palaeohorizontal, the limbs of these synformal structures therefore have a 40° dip from the horizontal.

Microstructures in the Skaergaard Layered Series *Plagioclase grain shape*

As first recognized by [Wager & Deer \(1939\)](#), the fabrics in the Skaergaard cumulates are predominantly defined by a plagioclase SPO (and associated CPO). Plagioclase mode decreases steadily through the floor cumulates of the Layered Series, from ~ 70 vol. % in the lowermost parts of the stratigraphy to ~ 30 vol. % in the most evolved cumulates ([Tegner *et al.*, 2009](#); [Holness *et al.*, 2015](#)). Plagioclase forms 'roughly square' tablets flattened parallel to (010) in the lower part of the

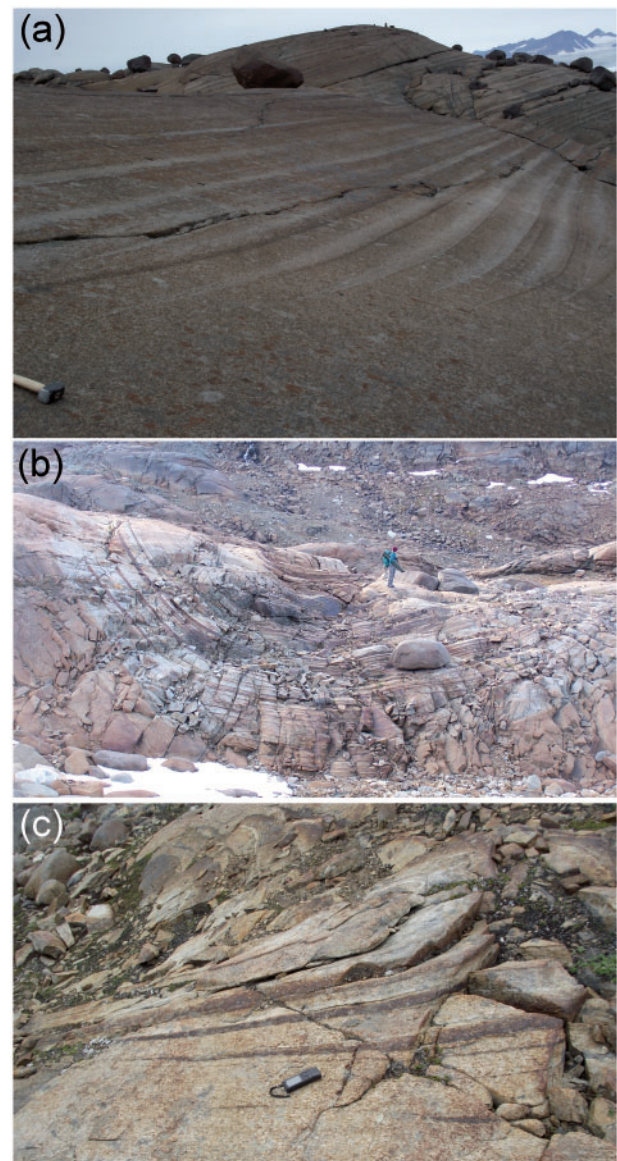


Fig. 3. Photographs of trough bands. (a) Trough band photographed looking south, with the intrusion margin to the left. Each modal packet comprises a melanocratic base grading abruptly into a leucocratic top. Each modal packet thins away from the trough band axis and is separated from the stratigraphically adjacent packets by average gabbro. (b) Trough band G photographed looking towards the intrusion centre (note figure for scale). The trough is marked by contiguous modal bands with a melanocratic base and leucocratic top (with no intervening average gabbro). (c) Trough band G photographed at the trough axis (which strikes from right to left, dipping to the left). (Note the thinning of the oxide-rich layers away from the trough axis.) Handheld GPS for scale.

stratigraphy ([Fig. 4a](#); [Wager & Deer, 1939](#)), becoming thicker and gradually elongated along [100] higher in the stratigraphy ([Wager & Deer, 1939](#); [Gay & Muir, 1962](#); [Nwe, 1975](#)). This change is manifest in thin section by a progressive reduction in the average apparent aspect ratio (AR) of the plagioclase, with grains appearing almost equant in thin-section in the more evolved horizons and with a significant proportion of grain intersections elongate perpendicular to the trace of the (010)



Fig. 4. Photomicrographs of the Layered series gabbros. All scale bars represent 2 mm. ol, olivine; cpx, Ca-rich clinopyroxene; ox, oxides; ap, apatite. (a) Sample 320'6'' from the upper part of LZa showing plagioclase tablets forming an SPO visible in thin section. (b) UZb sample 90/22 450 showing plagioclase with a low apparent aspect ratio. (c) LZa sample 458242 with randomly oriented plagioclase crystals and olivine enclosed by clinopyroxene oikocrysts. (d) LZb sample 458277. A noteworthy feature is the slight bending of the longer plagioclase crystals, which also contain discontinuous deformation twins; well-packed plagioclase crystals. (e) MZ sample 90/22-1035.03. (Note the wide range of apparent aspect ratio of the plagioclase and that the longer plagioclase crystals are bent.) (f) UZa sample 90/22-660 containing low aspect ratio plagioclase that is apparently randomly oriented (in the plane of the thin section).

twins (Fig. 4b) instead of the more usual elongation parallel to the twins (Holness, 2015). The progressive change in shape is thought to be a consequence of the response of the different growth faces to changes in cooling and crystallization rates, with the lowest values of AR found at the slowest-cooled horizons (Holness, 2014). Although Holness (2015) did not present data for the UBS, it is likely that the pattern observed in the Layered Series is mirrored at the roof: Wager & Brown (1968) stated that some parts of the UBS display a strong foliation parallel to the roof defined by the preferred alignment of highly tabular plagioclase (illustrated in their fig. 93, p. 134).

Foliations and lineations

The first detailed analysis of fabrics in the Skaergaard cumulates is that of Nicolas (1992), who documented a systematic SPO of plagioclase tablets creating a foliation defined by preferred alignment of (010) faces

dipping gently to the SE, together with lineations converging from the intrusion walls towards the SE. He interpreted all fabrics as magmatic (corresponding, in our classification, to primary fabrics). The strength of any preferred orientations, and the number of structures that he related to magmatic flow, decrease rapidly from the walls towards the intrusion centre. This, together with evidence for shearing (grain tilting, grain imbrication, oblique foliation), consistently with movement of the top towards the intrusion centre, led Nicolas (1992) to argue that the fabrics result from grain orientation in currents flowing from the walls onto an already consolidated floor. Although these arguments were repeated by McBirney & Nicolas (1997), Irvine *et al.* (1998) questioned the significance of their observations, arguing that because some lineations were measured in the syn-magmatic faults in the cross-bedded zone, and that other lineations are very weak, the fabrics might simply be the effect of a slight shifting

of the cumulate pile (i.e. they fall into our category of secondary fabrics).

At the stratigraphic level of the trough bands in UZ, plagioclase forms laths that are elongate along [100] (Gay & Muir, 1962; Nwe, 1975), and in the troughs themselves the plagioclase grains form a lineation clearly visible in outcrop, with their long axes aligned parallel to the axis of the trough (Wager & Deer, 1939; Nwe, 1975; it should be noted that Brothers (1964) erroneously stated that the elongation of the trough band plagioclase is along [001]). Olivine and pyroxene primocrysts (together with apatite primocrysts in some trough band layers) are also aligned with their long axes parallel to the trough axis, with the strongest alignment observed for the high aspect ratio apatite grains (Brothers, 1964). Irvine (1983) agreed with Wager & Deer (1939), Brothers (1964) and Nwe (1975) that these fabrics are a consequence of alignment in magma currents moving away from the intrusion walls.

Compositional zoning in Skaergaard plagioclase

Toplis *et al.* (2008) found that the rims of plagioclase crystals have a constant composition (An_{50}) from the base of the intrusion to lower MZ and argued that these rims grew during compositional convection within the mush. Humphreys (2009) investigated five samples from HZ, LZa, and LZb, in which plagioclase is predominantly normally zoned. She suggested that the rare examples of reverse zonation were the signature of localized dissolution–reprecipitation (i.e. compaction), but her subsequent work reported the presence of reverse zoning in rocks that are unlikely to have compacted (i.e. in the MBS, and in rocks containing high P_2O_5 concentrations). She suggested instead that the reverse zoned plagioclase crystallized from the Fe-rich conjugate of an immiscible interstitial liquid (Humphreys, 2011). Namur *et al.* (2014) took a closer look at the constant composition rims first documented by Toplis *et al.* (2008) and found that they change their composition with position in the stratigraphy; they attributed the rims to *in situ* growth in the mush during extended periods of near-isothermal crystallization. Zoning is generally parallel to the low index planes in the plagioclase.

Previous work on adcumulates and compaction in the Skaergaard intrusion

The bulk-rock concentration of P_2O_5 decreases upwards through the Layered Series until the arrival of primocryst apatite in UZb (Wager, 1963; Wager & Brown, 1968; McBirney, 1989a; Tegner *et al.*, 2009). This is argued to be a consequence of the amount of evolved interstitial liquid in the cumulates decreasing with increasing stratigraphic height; the floor cumulates are therefore argued to become more adcumulate with increasing stratigraphic height. Wager & Brown (1968) furthermore showed that, at any stratigraphic height below UZb, the bulk-rock P_2O_5 concentration is highest in

leucocratic layers and lowest in melanocratic layers. Critically, they noted that this difference is observed only if the leucocratic layers are not strongly foliated, and therefore attributed the difference to a greater original porosity in layers dominated by randomly oriented plagioclase. Their conclusion was essentially that the bulk-rock P_2O_5 concentration reflects packing efficiency (created during either primary or secondary fabric-forming events), with a looser and less efficient packing in rocks containing abundant and randomly oriented tabular grains.

The same correlation between mineral mode and bulk-rock P_2O_5 concentration was found on the metre-scale by Tegner *et al.* (2009) and Holness *et al.* (2015). Tegner *et al.* (2009) did not consider variations in fabric strength but argued instead that the correlation was a consequence of melanocratic layers compacting more than leucocratic layers. Compaction must thus have occurred in the uppermost few tens of meters of the mush, prior to the interstitial growth of apatite, K-feldspar, zircon and phlogopite. Tegner *et al.* (2009) argued for 'a hard-ground crystallization front with compaction to near-accumulates with a few per cent porosity and textural maturation within a few tens of metres of depth'. They did not discuss deformation mechanisms. McKenzie (2011) developed a model for viscous compaction in a progressively accumulating crystal pile, with particular application to the Skaergaard intrusion, using the bulk-rock compositional data of Tegner *et al.* (2009) to argue for compaction at the base of a 300 m thick mushy layer deforming by dislocation creep.

Two papers were published in 1997 arguing that the graded modal layering in the trough bands is a consequence of post-accumulation recrystallization driven by compaction. McBirney & Nicolas (1997) termed layering formed in this way 'compaction layering' and invoked the formation of the trough bands by localized (viscous) compaction, with the unlayered regions between the troughs being the uncompacted equivalents. Boudreau & McBirney (1997) suggested that the modal layering formed in a manner similar to that resulting in banding in metamorphic rocks, citing processes such as Ostwald ripening, pressure solution and self-organization driven by interfacial energy reduction, enhanced by mass redistribution by upwards-migrating liquids. Accordingly, the foliation in the trough bands formed by the rotation of (presumably originally randomly oriented) grains during compaction enhanced by differential dissolution and reprecipitation, associated with extensive static recrystallization and annealing. No mention was made in either study of the mineral lineations in the troughs.

ANALYTICAL METHODS

Electron backscatter diffraction analysis (EBSD)

After standard mechanical polishing using diamond paste down to $1/4 \mu\text{m}$ grit size, thin sections were polished for 1 h with $0.06 \mu\text{m}$ colloidal silica (SiO_2 particle

dispersion in an alkaline solution) at the University of Liverpool, UK. Seven samples were analysed using a tilted-column CamScan X500 CrystalProbe field emission gun (FEG) scanning electron microscope (SEM) at the University of Liverpool. Another five samples were analysed on a FEI sFEG XL30 SEM at the Department of Physics, University of Cambridge. All crystallographic datasets were collected, indexed and analysed using Oxford Instruments AZtec acquisition software, set to detect 12 bands, 120 Hough transform, 75 reflectors, at 2×2 binning and 2.7 s time per frame. Whole thin-section EBSD was carried out using a $20\text{-}\mu\text{m}$ step size, over an area of c. $20\text{ mm} \times 15\text{ mm}$. Each large map took 45 min acquisition time. Crystallographic information collected for six phases (olivine, plagioclase, enstatite, diopside, ilmenite and magnetite) is provided in [Supplementary Data Appendix 1](#) (supplementary data are available for downloading at <http://www.petrology.oxfordjournals.org>). EBSD maps and pole figures of crystallographic orientation were constructed using Oxford Instrument Channel 5 software, plotting one point per grain.

Channel 5 software permits the construction of maps of mineral phases, shape of grain intersections, and textural component maps. The phase map is determined using the crystallographic matching units of each constitutive phase. The shape map is constructed from the angle that the major axis of the best-fit ellipsoid of each grain intersection makes with the x -axis of the sample reference frame. Following [Britton *et al.* \(2016\)](#), the pole figure data are projected using an upper hemisphere, equal area projection. A review of this quantitative SEM technique has been given by [Prior *et al.* \(2009\)](#) and references therein.

QEMSCAN—quantitative evaluation of minerals by scanning electron microscopy

QEMSCAN images were obtained for 12 Skaergaard samples using a Quanta 650 F field emission gun equipped with two Bruker XFlash 6130 energy-dispersive spectrometers (EDS) at the Department of Earth Sciences, University of Cambridge. Further

information on the analysis has been given by [Holness \(2015\)](#). The QEMSCAN images were used to create Ca concentration maps to allow easy visualization of compositional zoning in plagioclase. Resolution of the QEMSCAN images is $5\text{ }\mu\text{m}$.

LOCATION AND CHOICE OF SAMPLES

We chose twelve samples through the Layered Series from existing collections (locations shown in [Fig. 2](#); with one sample chosen from the Cambridge 1966 drill core, and three from drill core 90/22, [Table 1](#)) for detailed microstructural analysis. This set includes nine samples chosen at random, with no regard given to the presence or absence of preferred mineral orientations visible in thin section or hand specimen. These samples have been previously described by [Holness *et al.* \(2007\)](#) and [Tegner *et al.* \(2009\)](#), and cover the full range of adcumulus character, with the calculated volume of trapped liquid decreasing from a maximum of 37.9 vol. % in the lowest sample, to a minimum of 3.0 vol. % in UZ ([Table 1](#); [Tegner *et al.*, 2009](#)). The nine samples are not oriented in the reference frame of the intrusion, although for samples far from the walls, any foliation or lineation is parallel, or close to parallel, to the intrusion floor at the time of formation. This means that although we can be certain of the orientation of any foliation relative to the intrusion, we cannot tell how any lineation is oriented within that foliation. For the purposes of this study, which is aimed at determining the strength and nature of fabrics and microstructures, this absence of absolute orientation information is not significant. We also chose three samples from trough band F (location shown in [Fig. 2](#)). The samples come from a single core drilled close to the axis of the trough, and are oriented with respect to the vertical.

MICROSTRUCTURE AND FABRICS IN THE SKAERGAARD LAYERED SERIES

In the following sections, we illustrate the various elements of the fabrics, using colour to pick out grains defining any SPO in thin-section maps. Fabrics defined

Table 1: Details of the Layered Series samples used for this study

Sample	Zone	Strat. height (m)	Mineral modes (vol. %)					Bulk-rock P_2O_5	Vol. % 'trapped liquid'	AR
			plag	ol	opx	cpx	oxides			
458242	LZa	381	33.7	21.9	7.5	36.3	0.4	0.12	37.9	2.98
320'6"	LZa	534	63.8	8.8	5.7	18.4	3.1			3.64
458227	LZb	898	44.6	25.2	5.9	23.1	1.2	0.06	14.2	3.36
458277	LZb	1310	59.6	3.7	0.4	32.3	3.9	0.03	6.1	2.75
458289	MZ	1613	52.0	—	—	36.1	11.5	0.02	2.8	2.30
SK84-363	MZ	1865	37.5	0.7	—	42.8	18.8			2.21
90/22-1035.03	MZ	1963	48.7	4.2	0.8	28.9	17.3			2.25
90/22-660.6	UZa	2322	51.7	12.9	—	29.9	5.4	0.04	3.0	1.92
90/22-450	UZb	2505	59.6	22.4	—	11.8	6.1			1.99

The scheme used to calculate the stratigraphic height is that of [Holness *et al.* \(2007\)](#), for which the zero point is the base of HZ. Mineral modes were determined using EBSD data. The bulk-rock P_2O_5 concentrations and the calculated trapped liquid are from [Tegner *et al.* \(2009\)](#). The average apparent aspect ratio, AR, is taken from [Holness \(2015\)](#), or measured as part of this study.

by a CPO are illustrated using EBSD data to create pole figures. Importantly, whereas we can always detect a CPO using EBSD on a randomly oriented thin section, the detection of an SPO is possible only if the thin section is suitably oriented: for this study, we chose thin sections that were oriented randomly in rocks with no visible fabrics, but in rocks with a clearly visible SPO-defined fabric the thin sections were oriented perpendicular to this fabric. The average apparent aspect ratio of the plagioclase (as viewed in thin section), AR, is dependent not only on the strength of any preferred orientation but also on the orientation of the thin section relative to the fabric: although we report the values of AR in our thin sections (Table 1), we do so simply for descriptive purposes.

Critically, the matching of CPOs with SPOs, and their interpretation as either foliations or lineations, is dependent on us knowing grain shape. For example, for tabular plagioclase grains flattened on (010) a foliation is manifest in a pole figure by the poles to both (100) and (001) forming a girdle perpendicular to a single point maximum of poles to (010) (Fig. 5a). However, if the grains were rod-like, a similar set of pole figures comprising two girdles and a point maximum would denote an SPO lineation (Fig. 5b).

Lower Zone A (LZa)

Two samples were chosen from LZa, in which the cumulus phases are olivine and plagioclase, with interstitial augite, inverted pigeonite and Fe–Ti oxides. In the stratigraphically lowest sample (458242) plagioclase is commonly enclosed by clinopyroxene oikocrysts

(Fig. 4c). The enclosed plagioclase grains are generally significantly smaller than those outside the oikocryst (Fig. 4c). Plagioclase crystals are oriented in three directions: either subparallel to the γ -direction of the sample reference frame (green grains in Fig. 6a); sub-orthogonal to the γ -direction (red grains, Fig. 6a); or parallel to the γ -direction (yellow grains, Fig. 6a). There is no strong CPO (Fig. 6b). The (010) planes of the subparallel and the sub-orthogonal plagioclase crystals are almost 90° apart (Fig. 6c).

Sample 320'6'', from the top of LZa, contains elongate, well-aligned plagioclase crystals with high AR (Table 1), together with commonly rounded but sometimes elongate olivine primocrysts (Fig. 4a). Clinopyroxene is interstitial, but not oikocrystic (Fig. 4a). Alignment of (010) planes of the tabular plagioclase creates a strong foliation (green and yellow crystals, Fig. 6d), shown by the strong point maximum of (010) with a perpendicular girdle distribution of [100] and (001) (Fig. 6f). Some comparatively equant crystals lie orthogonal to the foliation (red crystals, Fig. 6d).

Olivine in sample 458242 is randomly oriented (Fig. 7a and b), and insufficient grains were present in 320'6'' to generate a meaningful pole figure. The low number of clinopyroxene crystals in 458242 also prevents a statistically meaningful assessment of CPO. The more abundant clinopyroxene in 320'6'' shows a weak CPO foliation, with [001] axes distributed as a girdle parallel to the foliation defined by plagioclase (010) planes, a point maximum at (100) and a poor girdle distribution of (110) (Fig. 7c and d).

In sample 320'6'' (LZa), plagioclase crystals exhibit lattice distortion up $\sim 10^\circ$, and are locally bent around

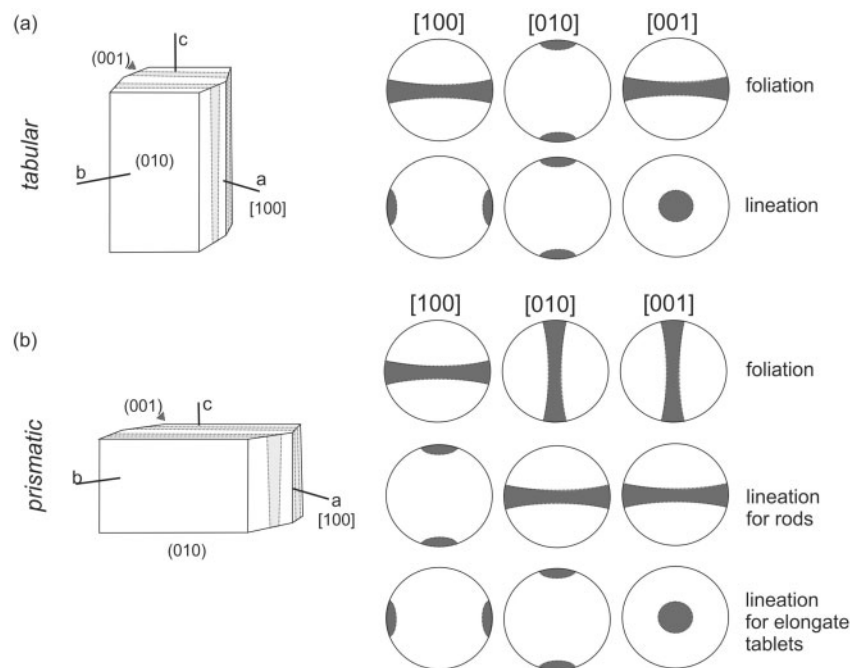


Fig. 5. Schematic illustrations showing the expected pole figures for foliations and lineations as a function of plagioclase grain shape for (a) tabular plagioclase, and (b) elongate prisms and rods.

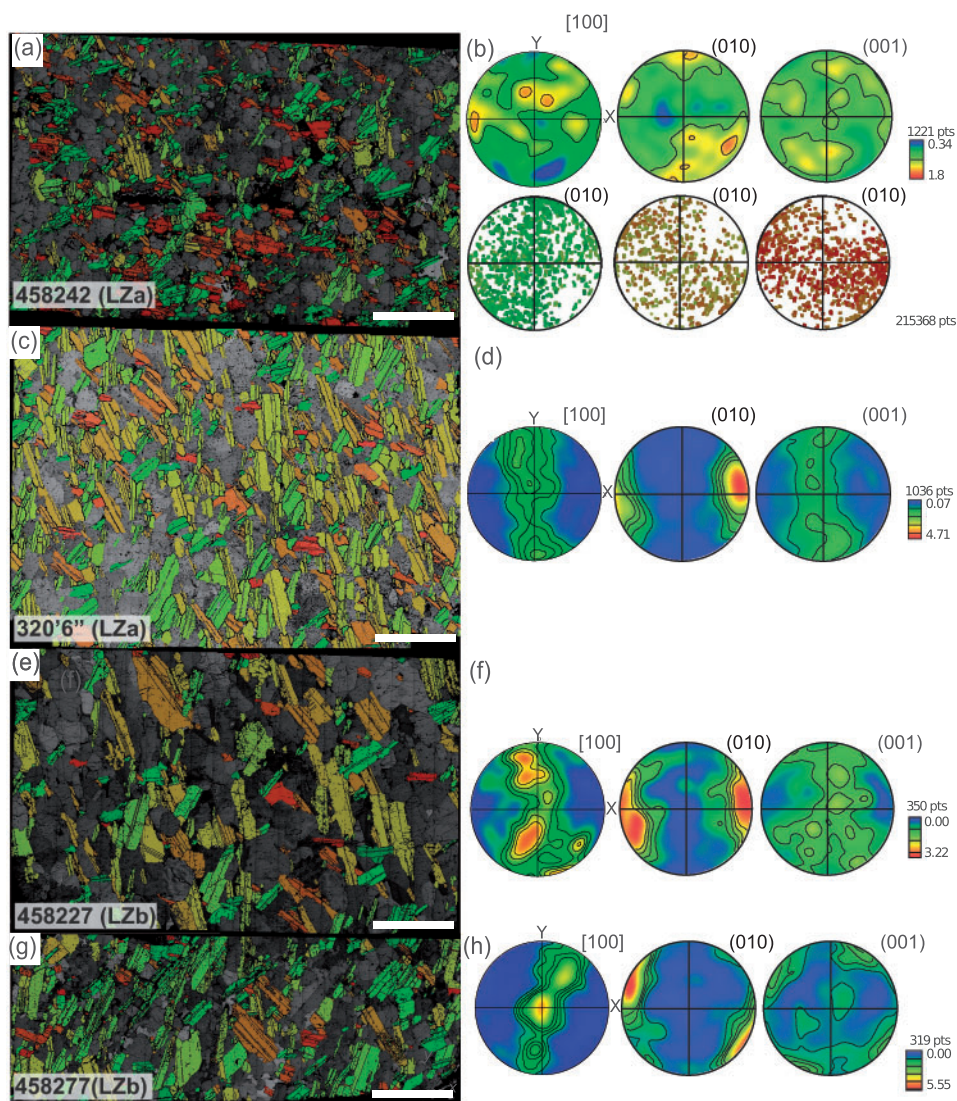


Fig. 6. Plagioclase orientation and grain shape data. The grain shape maps were constructed using the orientation of the major axis of the best-fitted ellipsoid and the pole figures were plotted with one point per grain. (a) Grain shape map for LZa sample 458242 and (b) the corresponding density contour plot of the pole figure data, plotted as one point per grain, together with the (010) pole figure data of three plagioclase subsets subdivided according their grain shape orientation as shown in (a). (c) Grain shape map for LZa sample 320'6'' and (d) the corresponding density contour plot of the pole figure data. (e) Grain shape map for LZb sample 458227 and (f) the corresponding density contour plot of plagioclase pole figures. (g) Grain shape map for LZb sample 458277 and (h) the corresponding density contour plot of the pole figure data. For all contour plots half-width is 20° and data clustering is 10° .

other grains. Olivine grains contain some low-angle boundaries as well as internal lattice distortion of up to $\sim 8^\circ$. The qualitative QEMSCAN maps reveal that plagioclase crystals in both LZa samples are normally zoned, with a sharp transition between cores and rims parallel to both (010) and (001) faces (Fig. 8a).

Lower Zone B (LZb)

We examined two samples from LZb, in which olivine, plagioclase and clinopyroxene are cumulus phases, whereas Fe–Ti oxides are interstitial. In both samples 458227 and 458277, the (010) planes of tabular plagioclase form a foliation defined by a broad point maximum of poles to (010), a perpendicular girdle distribution of [100] parallel to the foliation and a much weaker girdle of (001) (Fig. 6e–h). In 458277, the pole figure for (001)

contains a point maximum parallel to that of (010) in addition to the very weak girdle (Fig. 7h): the CPO for this sample is very similar to those seen in the two overlying MZ samples (see next section). The foliation is visible in thin section as an SPO defined by the high AR yellow and orange crystals (Fig. 6e and g). Relatively equant grains are oriented at an angle to this foliation.

In both LZb samples, olivine cumulus grains are elongate in thin section and are weakly aligned parallel to the plagioclase foliation, although insufficient grains were present to generate a meaningful pole figure. The few elongate crystals of clinopyroxene in sample 458227 (orange crystals, Fig. 7e) are weakly aligned to the plane of the plagioclase-defined foliation, associated with a weak CPO with a diffuse point maximum for the [001] axis and (100) plane (Fig. 7f). In sample

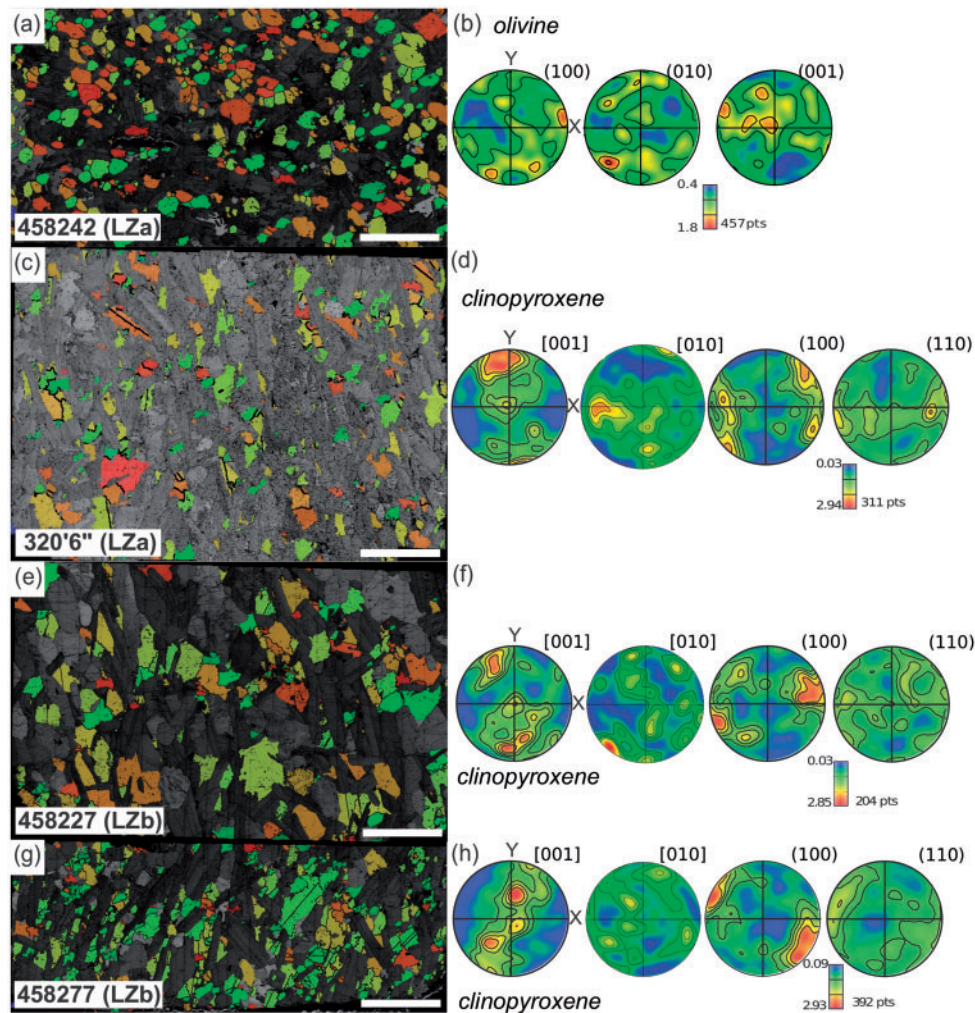


Fig. 7. Olivine and clinopyroxene orientation and grain shape data. The grain shape maps were constructed using the orientation of the major axis of the best-fitted ellipsoid as viewed in thin section, and the pole figures were plotted with one point per grain. (a) Olivine grain shape maps for LZa sample 458242, together with (b) the density contour plot of the pole figure data. (c) LZa sample 320'6'' showing the clinopyroxene grain shape map and (d) the density contour plot of the pole figure data. (e) LZb sample 458227 showing the clinopyroxene grain shape map and (f) the density contour plot of the pole figure data. (g) LZb sample 458277 showing the clinopyroxene grain shape map and (h) the density contour plot of the pole figure data. For all contour plots half width is 20° and data clustering is 10° .

458277, clinopyroxene displays a stronger SPO, with most grains oriented with their major axes parallel to the (plagioclase-defined) foliation (Fig. 7g and h). Comparison of the CPO with that of plagioclase suggests that the clinopyroxene grains are flattened along (100), and elongate along [001].

Highly tabular plagioclase commonly contains deformation twins and $2\text{--}5^\circ$ low-angle boundaries: single grains may be distorted by up to 5° (Fig. 4d). In contrast, the internal deformation in olivine grains reaches a maximum of only a few degrees. Both LZb samples contain normally zoned plagioclase crystals, with zoning along both (010) and (001) faces (Fig. 8b).

Middle Zone (MZ)

We examined three samples from MZ, in which the cumulus phases are plagioclase, clinopyroxene, Fe–Ti oxides and orthopyroxene, with olivine present only as

rims surrounding Fe–Ti oxide grains. Plagioclase in samples 458289 and SK84-363 appears moderately elongate in thin section with an SPO defined by weak alignment of the elongate grains (Fig. 9a–d). Those crystals aligned with their apparent long axis orthogonal to this SPO generally have relatively low apparent aspect ratios. The CPOs in these two samples are similar, with a preferred alignment of plagioclase (010) forming a strong point maximum, the [100] axis forming a girdle distribution orthogonal to (010) with a notable diffuse point maximum, whereas poles to (001) are intermediate between a girdle similar to that of [100] and a point maximum similar to that of (010) (Fig. 9b and d). Sample 90/22-1035.03, from the top of MZ, shows only a weak SPO in the thin section we examined (Fig. 9e). The CPO in 90/22-1035.03 is characterized by the same girdle containing a point maximum for [100] that is present in the other two MZ samples (and the topmost

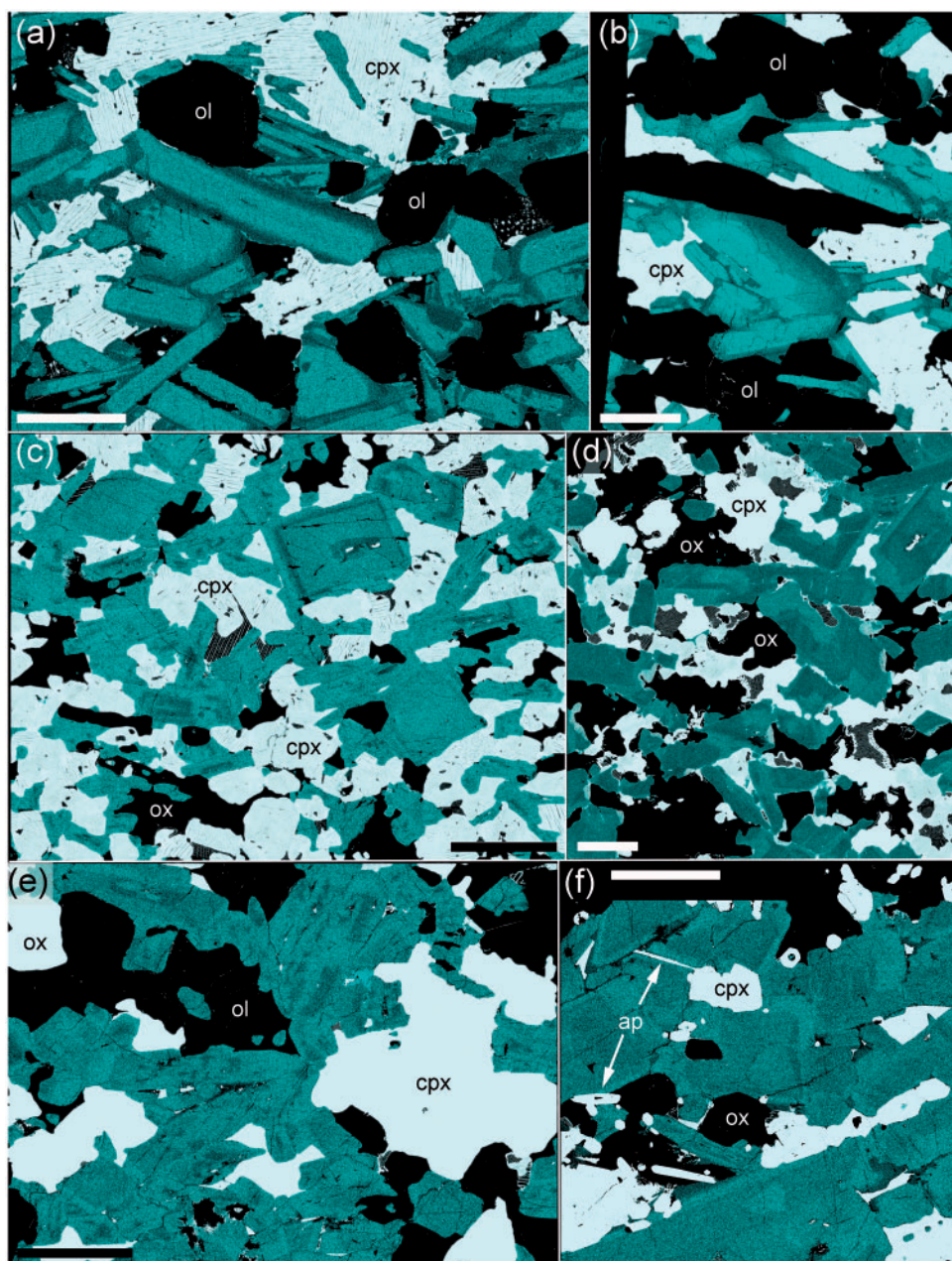


Fig. 8. QEMSCAN maps of Ca distribution, showing compositional zoning in plagioclase. Plagioclase is blue–green, with the darker colours denoting relatively sodic compositions. Mineral abbreviations for minerals other than plagioclase as in Fig. 4. Scale bars represent 2 mm. (a) LZa sample 320'6''. (b) LZb sample 458227. (c) MZ sample SK84-363. (d) MZ sample 90/22-1035.03. (e) UZa sample 90/22-660.6. (f) UZb sample 90/22-450.

LZb sample), and a very weak point maximum for (010) that is transitional to a girdle at a high angle to the [100] point maximum (Fig. 9f). The pole figure for (001) is very similar to that of (010).

Cumulus clinopyroxene appears elongated in the three MZ thin sections (Fig. 10a, c and e), and is oriented with the (100) planes parallel to plagioclase (010). In thin section, sample 458289 is characterized by two dominant orientations of the long axis, both of which are subparallel to the plagioclase-defined foliation plane but with slightly different angle (green and red grains, Fig. 10a). The clinopyroxene pole figure for

sample 458289 shows a strong CPO with a girdle distribution of the [001] axes, a strong point maximum of the poles to the (100) plane and a dispersed point maximum for [010] and poles to the (110) plane (Fig. 10b). Sample SK84-363 is characterized by a dispersed point maximum of [001] and a strong point maximum of (100) planes (Fig. 10d). [010] axes and poles to (110) have distributions that are transitional between point maxima and girdle (Fig. 10d). In contrast, clinopyroxene in sample 90/22-1035.03 is randomly oriented (Fig. 10f).

Some plagioclase grains, particularly those that are highly elongate in thin section, show evidence of crystal

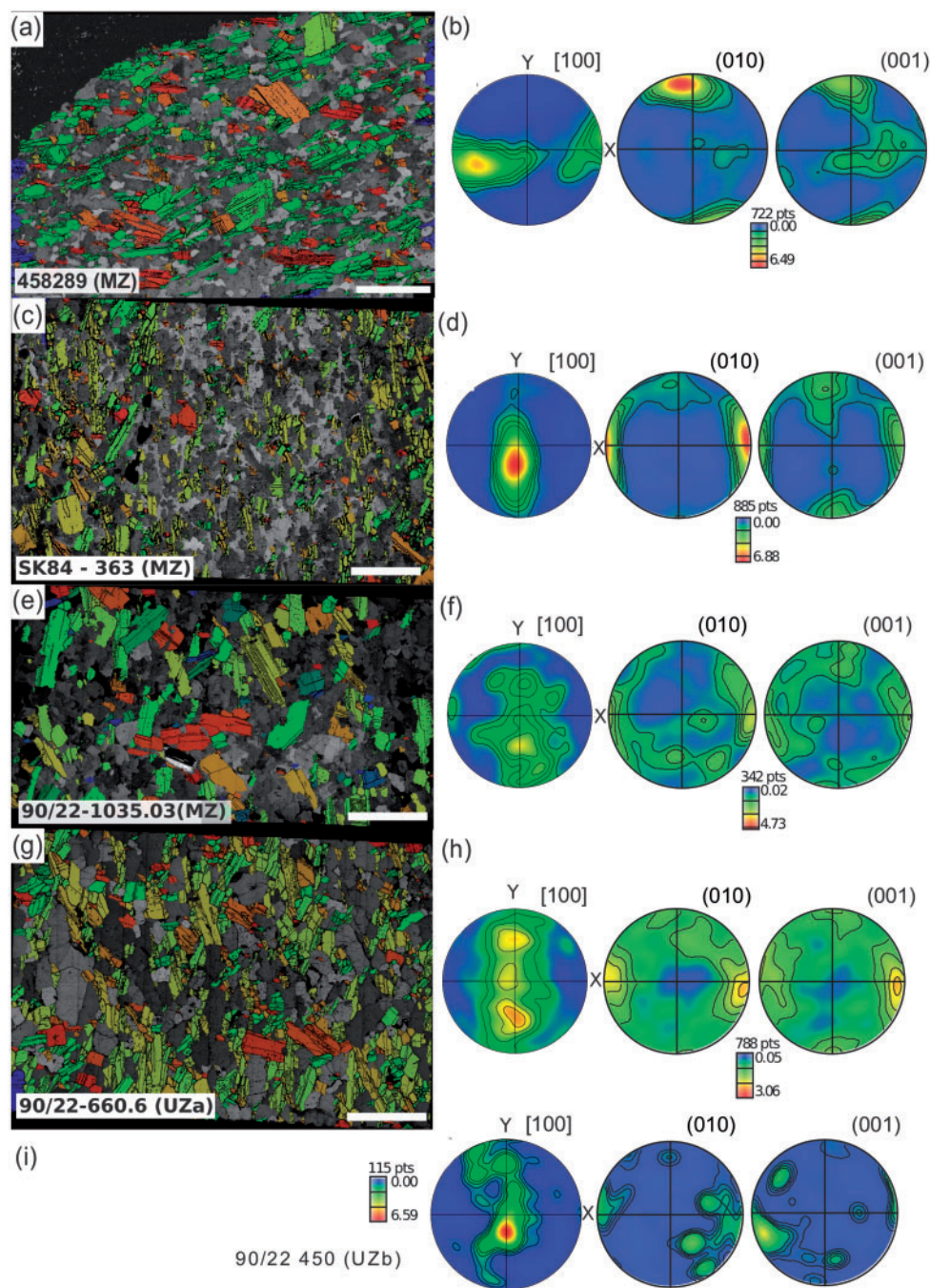


Fig. 9. Plagioclase orientation and grain shape data. The grain shape maps were constructed using the orientation of the major axis of the best-fitted ellipsoid as viewed in thin section and the pole figures were plotted with one point per grain. (a) Grain shape map for MZ sample 458289 and (b) the corresponding density contour plot of the pole figure data. (c) Grain shape map for MZ sample SK84-363 and (d) the corresponding density contour plot of the pole figure data. (e) Grain shape map for MZ sample 99/22-1035.03 and (f) the corresponding density contour plot of plagioclase pole figures. (g) Grain shape map for UZa sample 90/22-660.6 and (h) the corresponding density contour plot of the pole figure data. (i) UZb sample 90/22-450 showing the pole figure data for plagioclase. For all contour plots half width is 20° and data clustering is 10° .

plasticity (Fig. 4e). In sample SK84-363, both plagioclase and clinopyroxene contain numerous low-angle boundaries. Plagioclase lattices are distorted by up to $\sim 5^\circ$, with complex low-angle boundaries angled by 2° , whereas lattice distortion within clinopyroxene is up to 15° . Plagioclase is either normally, reversed or oscillatory zoned (Fig. 8c), but the zoning is always parallel to

low-index faces. There are some complex zoning patterns in the centres of some grains (Fig. 8c and d).

Upper Zone A (UZa) and Upper Zone B (UZb)

We examined two samples from UZ, in which plagioclase, olivine, clinopyroxene and Fe–Ti oxides are cumulus (with the addition of apatite in UZb).

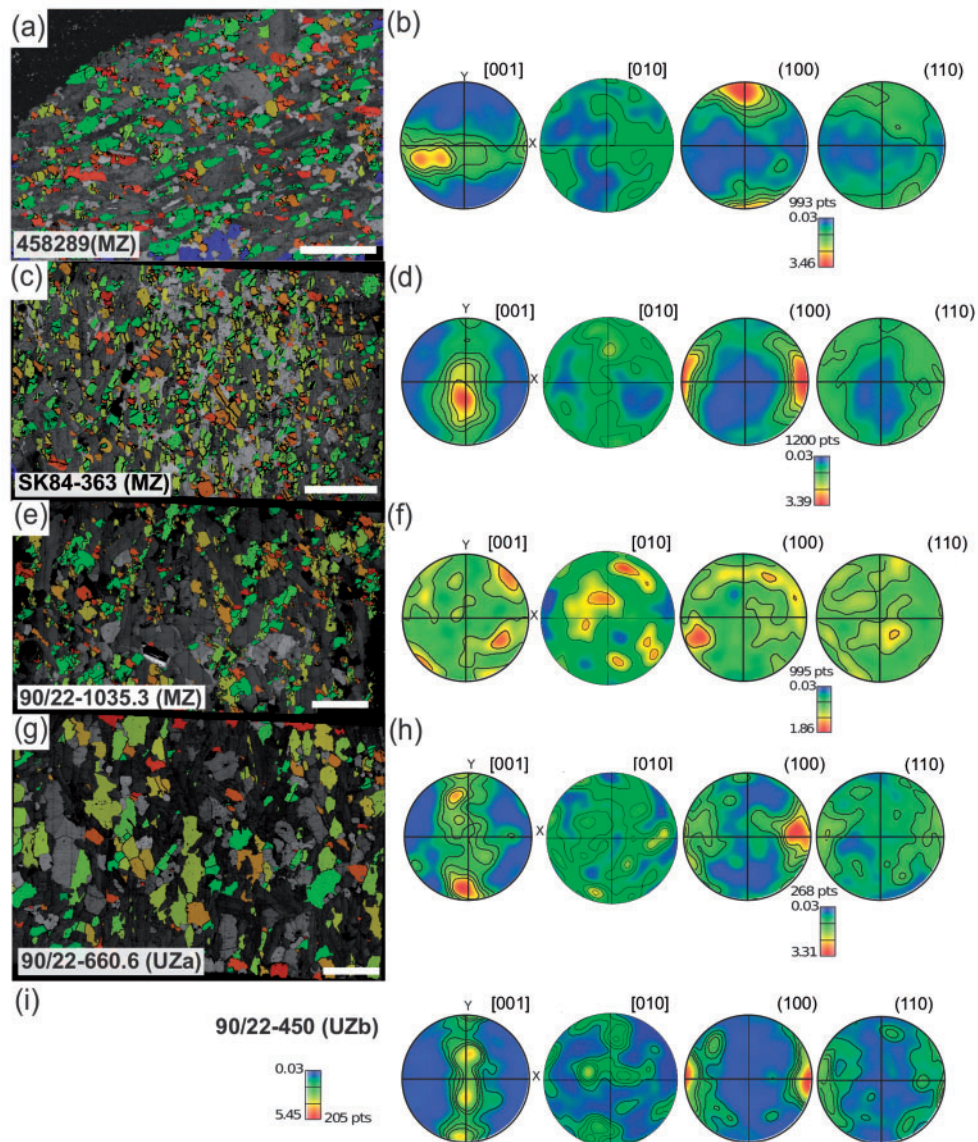


Fig. 10. Clinopyroxene orientation and grain shape data. The grain shape maps were constructed using the orientation of the major axis of the best-fitted ellipsoid as viewed in thin section, and the pole figures were plotted with the orientation of the major axis of the best-fitted ellipsoid as viewed in thin section, and the pole figures were plotted with one point per grain. (a) MZ sample 458289 grain shape map with (b) the corresponding density contour plot of the pole figure data. (c) MZ sample SK84-363 showing grain shape data and (d) the corresponding density contour plot of the pole figure data. (e) MZ sample 90/22-1035.3 showing the clinopyroxene grain shape map and (f) the corresponding density contour plot of the pole figure data. (g) UZa sample 90/22-660.6 showing clinopyroxene grain shape map and (h) the corresponding density contour plot of the pole figure data. (i) UZb sample 90/22-450 showing the pole figure data for clinopyroxene. For all contour plots half width is 20° and data clustering is 10° .

Plagioclase has low AR in thin section (Table 1) and there is no clear SPO visible in the thin sections we examined (Fig. 4b and f). Olivine is generally rounded and subhedral, whereas clinopyroxene primocrysts are commonly significantly elongated.

In both UZ samples a weak plagioclase CPO forms coincident diffuse point maxima for (010) and (001), and a girdle distribution of [100] with a diffuse point maximum. This is most evident in UZa sample 90/22-660.6 (Fig. 9h), as poor indexing of plagioclase in the UZb sample 90/22-450 led to a small dataset (Fig. 9i).

Whereas the clinopyroxene [010] axes show no preferred orientation, the clinopyroxene CPO comprises a

girdle distribution of the [001] axis (parallel to the girdle of plagioclase [100]), a strong point maximum of (100) planes and a slightly weaker point maximum of (110) planes (both parallel to the plagioclase (010)) (Fig. 10h and i). This matching of the two minerals implies a similar SPO. There is insufficient olivine to constrain the CPO.

The UZa sample contains little evidence for crystal plasticity, with most of what little strain is present in plagioclase and clinopyroxene. Plagioclase contains 2° low-angle boundaries and lattice distortion of $\sim 5^\circ$. Clinopyroxene locally contains (commonly curved) low-angle boundaries. Plagioclase in the UZ samples

contains patchy reverse zoning but, where present, the Ca-rich rims can be traced along all growth faces (Fig. 8e and f).

Trough band samples (UZa)

The three UZa samples from trough band F are predominantly from the plagioclase-rich component of the modal layers. They contain low AR plagioclase grains with well-developed crystal faces. In the transitional region between the mafic and felsic parts of the modal layers, olivine, clinopyroxene and Fe–Ti oxides are interstitial phases (Figs 11a, b and 12a). In the middle parts of the felsic layers, quartz and minor K-feldspar are the interstitial phases (Figs 11c and 12b). In the melanocratic parts of the modal layers, the plagioclase grains are rounded where surrounded by oxide (Fig. 12c).

The low apparent aspect ratio of the plagioclase in our thin sections results in weak or absent SPO. In contrast, there is a well-defined CPO in all three samples, in which [100] forms a distinct point maximum (Fig. 13). In samples 118916 and 118918, (001) and (010) form a weak girdle orthogonal to the [100] axes (Fig. 13b and f); in sample 118917, (010) and (001) form weak point maxima approximately orthogonal [100] (Fig. 13d).

Compositional zoning is not well developed in the plagioclase, although normal zoning is present along plagioclase faces in contact with interstitial quartz: simultaneous growth of the plagioclase and the interstitial quartz is shown by the small-scale irregularities of the plagioclase margins (Figs 11c and 12b). Some grains show well-developed oscillatory zoning parallel to low-index growth faces. There is almost no evidence for intra-crystalline deformation in the trough band samples: only a few deformed grains were found in the several thin sections we examined (e.g. Fig. 11b).

DISCUSSION

From our own experience and from comparison of published photomicrographs and petrographic descriptions, the fabrics and microstructures observed in our sample set are typical of those found in the great majority of Skaergaard Layered Series gabbros. The following discussion can therefore be extended more generally to the Layered Series.

The fabrics in the gabbros from the lower part of the Layered Series (with the exception of the lowest sample) have a clear association between an SPO (foliation) defined by the alignment of tabular plagioclase and a CPO defined by a point maximum for poles to (010) and a girdle distribution of both [100] and [001]. This is exemplified by samples 320'6'' and 458227, and corresponds to the 'axial-B' CPO of Satsukawa *et al.* (2013), which is ascribed to crystal alignment during magmatic flow (i.e. our primary and secondary fabric

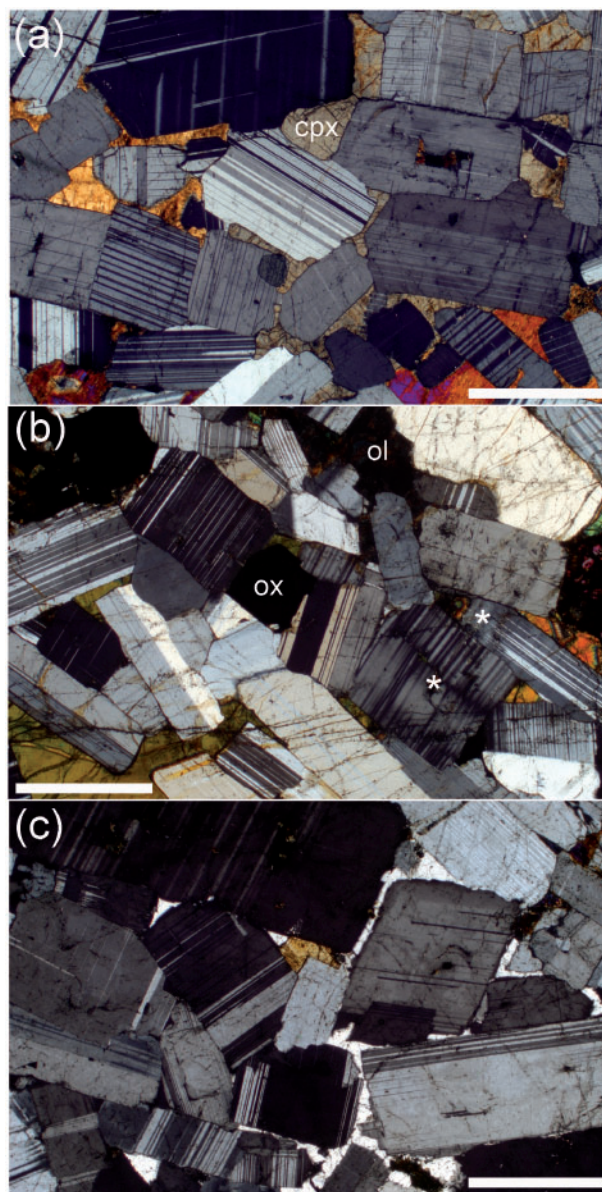


Fig. 11. Photomicrographs of trough band F. All scale bars represent 1 mm. (a, b) The low aspect ratio and euhedral shape of the cumulus plagioclase grains should be noted. The transitional region between the mafic and felsic parts of the modal layers is characterized by interstitial olivine, clinopyroxene and Fe–Ti oxides. The two grains in (b) marked with asterisks contain bent lattices and deformation twins. (c) In the middle parts of the felsic layers, quartz and minor K-feldspar are the interstitial phases. The normal zoned margins to the plagioclase where in contact with quartz should be noted.

formation stages). There is a consistent trend from this clearly defined fabric upwards in the stratigraphy to a CPO defined by poles to both (010) and (001) being aligned with each other but perpendicular to the alignment of [100]: this corresponds to the 'type-P' fabric of Satsukawa *et al.* (2013). The type-P CPO is found in oceanic gabbros in which the magmatic fabric has been obliterated by recrystallization during plastic deformation resulting in what Satsukawa *et al.* (2013) described as mylonitic microstructures (their fig. 2): this

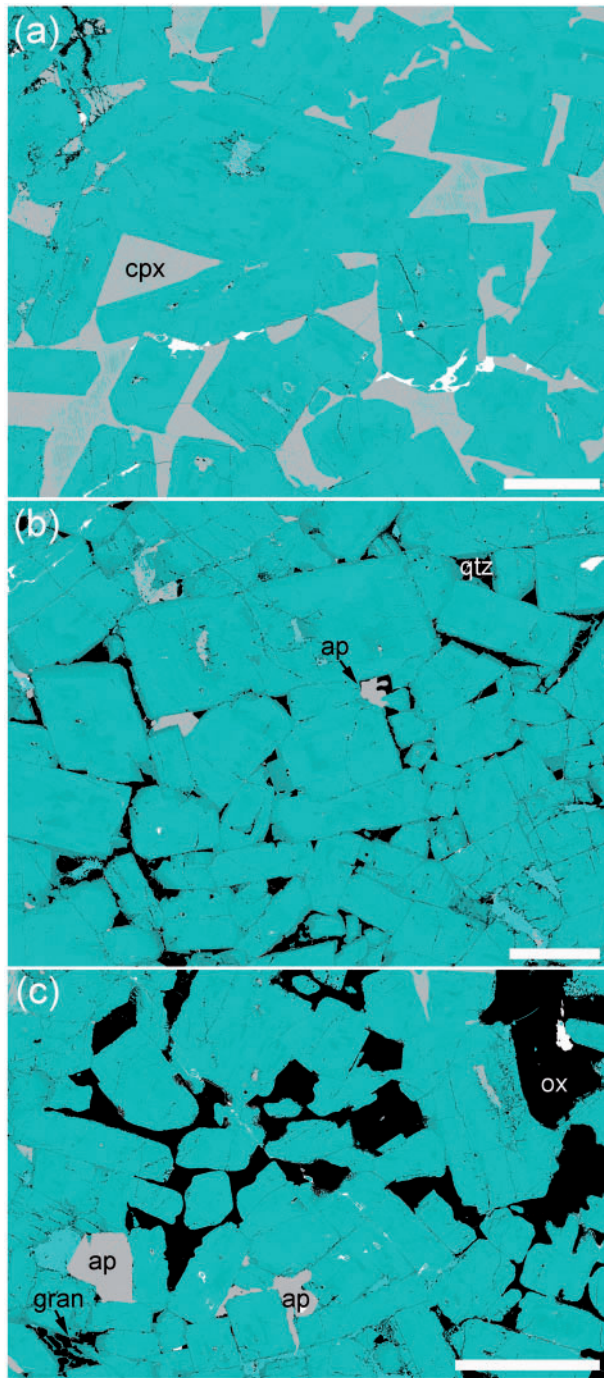


Fig. 12. QEMSCAN images of trough band F samples, showing plagioclase as blue–green, with darker colours denoting albitic compositions. (a) Basal part of the plagioclase-rich band contains interstitial clinopyroxene (grey in this image). The very sharp, planar margins of the euhedral plagioclase should be noted. Scale bar represents 1 mm. (b) The upper part of the plagioclase-rich layer contains interstitial quartz (black in this image): the plagioclase has albitic margins where in contact with quartz. Scale bar represents 1 mm. (c) Plagioclase is rounded where surrounded by interstitial oxides (black in this image) at the base of the plagioclase-rich layer. The interstitial apatite (ap) and granophyre (gran) should be noted. Scale bar represents 2 mm.

corresponds to a tertiary fabric according to our scheme and was attributed to dislocation creep on the (010)[100] slip system (Satsukawa *et al.*, 2013). In contrast, the Skaergaard gabbros with this CPO show almost no signs of recrystallization or plastic deformation attributable to dislocation creep (Figs 4e, f and 11a–c). Instead, in a similar manner to the foliation in the lower parts of the stratigraphy, the CPO fabric in the upper parts of the stratigraphy appears to be associated with an SPO, mirrored in the preferred alignment of non-equant cumulus grains of olivine and clinopyroxene.

If the type-P CPO in the Skaergaard UZ is a foliation, the point maximum for [100] would imply a fabric formed by the preferred alignment of tablets flattened perpendicular to [100]. This shape is not observed for plagioclase in igneous rocks. Instead we suggest that the gradual change in the CPO up through the stratigraphy is associated with the change towards the elongation along [100] described by Wager & Deer (1939), Gay & Muir (1962) and Nwe (1975), and a reduction of the flattening along (010) as plagioclase becomes less tabular and more prismatic (e.g. Fig. 5), manifest by the steady stratigraphic evolution of AR (Holness, 2015). Accordingly, the fabric in 90/22-1035.03 (the uppermost MZ sample) is a foliation in which plagioclase prisms elongate along [100] are weakly lineated. In both UZ samples (particularly 90/22-660.6, as poor indexing in 90/22-450 led to a small dataset), the CPO in these two samples is a stronger version of that seen in the uppermost MZ sample, continuing the gradual evolution up through the stratigraphy from a clear foliation defined by a preferred orientation of plagioclase grains flattened on (010) to a fabric defined by parallelism of poles to both (010) and (001), which are perpendicular to a preferred alignment of [100]. We interpret the fabric as an alignment of prismatic plagioclase elongated along [100], in which either the (010) faces or (less commonly) the (001) faces lie in the plane of the foliation (i.e. the faceted grains generally lie so that one or other of these two faces, most commonly (010), is in the plane of the foliation), with a weak lineation created by preferred alignment of the elongate [100] axes in the plane of the foliation. This fabric reaches its greatest expression in the trough band samples, where the CPO is consistent with a lineation oriented almost perpendicular to the plane of the thin section, explaining both the absence of a visible SPO in our thin sections and the clearly visible SPO lineation in outcrop.

The role of dislocation creep in the formation of the Skaergaard adcumulates

The set of nine Layered Series samples contain some evidence of bending of single grains, low-angle boundaries and lattice distortion in plagioclase, olivine and clinopyroxene (Fig. 4), regardless of whether it is cumulus or interstitial. Low-angle boundaries are uncommon, and the dominant intra-grain microstructure is

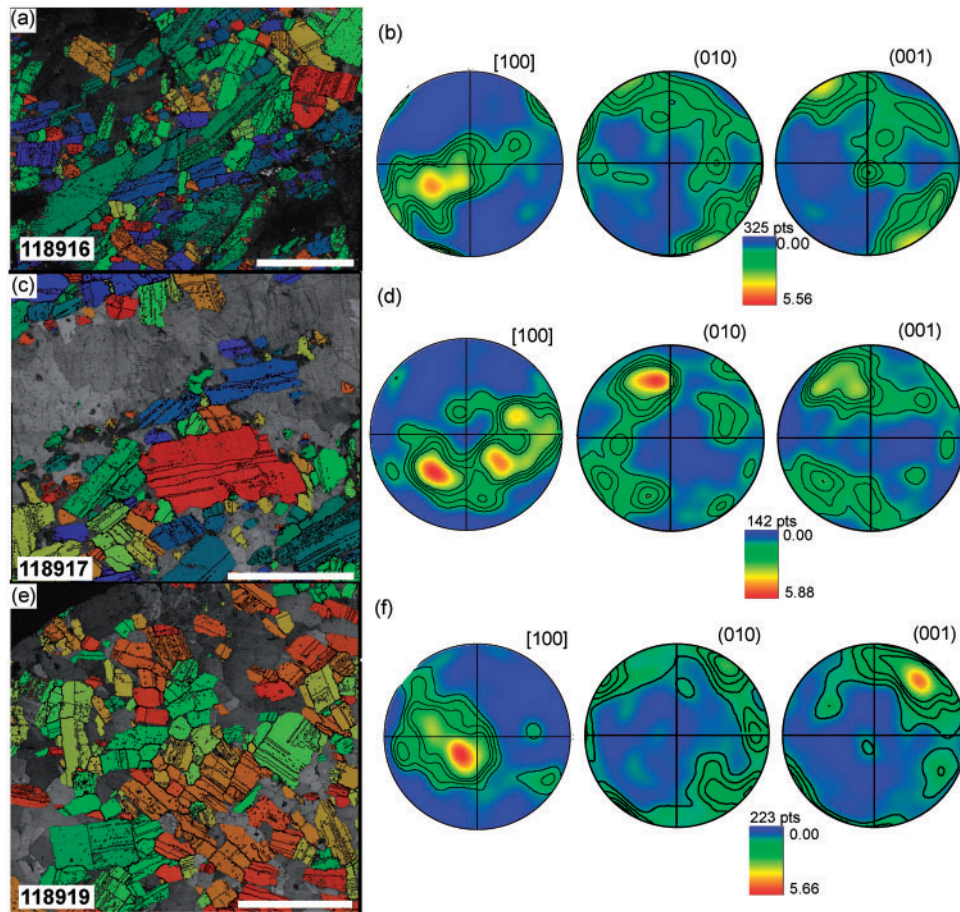


Fig. 13. Fabrics in the trough bands, with the grain shape maps constructed on the basis of the orientation of the major axis of the best-fitted ellipsoid as viewed in the thin section and pole figures plotted as one point per grain. (a) Plagioclase grain shape map for sample 118916 and (b) the corresponding density contour plot of the pole figure data. (c) Plagioclase grain shape map for sample 118917 and (d) the corresponding density contour plot of the pole figure data. (e) Plagioclase grain shape map for the sample 118919 and (f) the corresponding density contour plot of plagioclase pole figure. For all contour plots half width is 20° and data clustering is 10° .

lattice distortion manifest as undulose extinction caused by the bending of plagioclase crystals (Fig. 4). Overall, the nine samples record a similar (small) amount of strain, regardless of the bulk-rock P_2O_5 concentration and the calculated fraction of trapped liquid. The almost complete absence of low-angle grain boundaries in the trough band samples (Fig. 11) eliminates all possibility of the lineation (and, by extension, the modal layering) resulting from recrystallization during dislocation creep. Furthermore, although it is not clear which of the many olivine slip systems would be active under the conditions experienced by the crystal mush on the Skaergaard chamber floor, our olivine orientation and misorientation data are not consistent with the operation of dislocation creep (i.e. there is no evidence of lattice distortion or recrystallization of olivine).

The expulsion of interstitial liquid cannot have been achieved entirely by viscous compaction via dislocation creep. Instead it is only possible to argue that some compaction may have occurred equally through the Layered Series, resulting in very minor plastic deformation, with only a minimal effect on the final volume of interstitial liquid.

The role of dissolution–reprecipitation in the formation of the Skaergaard adcumulates

In our sample set, plagioclase grains commonly form two groups: the preferred orientation of (010) planes of the dominant group defines the foliation, whereas the (010) planes of the other group (crystals coloured red, Figs 6 and 9) are orthogonal to sub-orthogonal to the foliation. These orthogonal grains generally have relatively low apparent aspect ratio and are small. Such variation may be caused by a control of orientation on growth kinetics: it is also consistent with ‘unfavourably’ oriented grains undergoing dissolution and/or hindered growth during compaction (see Meurer & Boudreau, 1998). However, there are several reasons why we think this is not the case.

First, the Meurer & Boudreau (1998) model predicts that adcumulates should be those rocks that have the strongest foliations and highly tabular plagioclase. In contrast, the Layered Series plagioclase becomes less tabular, with weaker CPO (and associated SPO), with stratigraphic height, creating an anti-correlation between average apparent aspect ratio, fabric strength and the extent of adcumulate character (Table 1). At

least part of this lack of correlation may be because it is likely that plagioclase is unable to form a strong fabric in cumulates containing significant amounts of other primocryst phases: the Skaergaard gabbros contain a maximum of 70 vol. % plagioclase, whereas the Meurer & Boudreau dataset was obtained from anorthosites and anorthositic troctolites. However, whereas it might be argued that compaction could have been achieved by the preferential dissolution–reprecipitation of phases other than plagioclase, there is nothing known about anisotropic behaviour of olivine or clinopyroxene. Furthermore, the known anisotropy of dissolution in plagioclase (at least in hydrous fluids) would produce a fabric with an elongation of grains perpendicular to the trace of the (010) twins instead of the observed fabric parallel to the twins.

Second, the compositional zoning in the Skaergaard samples is consistent with interstitial growth on all plagioclase faces (Figs 8 and 12b), entirely unlike that expected for dissolution–reprecipitation. This is particularly the case for the concentric oscillatory zoning observed in the adcumulates of MZ (Fig. 8c and d) and trough band samples, in which plagioclase grain shapes are defined by planar, low-index growth faces consistent with a crystal shape created during growth under liquid-rich conditions (Figs 11 and 12). These features cannot be explained by dissolution–reprecipitation under uniaxial stress (Fig. 1). The modal banding in the trough bands must be an original magmatic feature and cannot have resulted from recrystallization during compaction: the corollary of this conclusion is that the homogeneous gabbros of UZ also could not have undergone compaction.

A definitive resolution of the absence of agreement between this study and the data of Meurer & Boudreau (1998) requires an understanding of the anisotropy of dissolution for the common primocryst phases in silicate melt. In the meantime, it is worth considering the comment of Brown (1956) that, for an accumulation of non-equant plagioclase grains, further growth can only result in an increase of aspect ratio for those grains that begin by having their (010) faces in contact: a crystal pile with a strong (primary) foliation will become a rock containing plagioclase with a much higher aspect ratio than a fully solidified crystal pile comprising grains with the same starting shape but a weaker foliation. The correlation between apparent aspect ratio and foliation strength observed by Meurer & Boudreau (1998) may thus be a consequence of overgrowth of primary accumulations with a variable initial fabric strength.

The origin of fabrics in the Skaergaard gabbros

The evidence presented above supports the interpretation of the fabrics in the Skaergaard gabbros as a record of processes occurring either during crystal accumulation or by rearrangement at the interface between the mush and the bulk magma by the action of magmatic currents: they are either primary or secondary fabrics.

The correlation between the CPO of interstitial clinopyroxene and that of cumulus plagioclase in LZa (Figs 6d and 7d) might indicate oriented heterogeneous nucleation and growth as suggested by Mainprice & Nicolas (1987), Godard & Van Roermund (1995) and Mauler *et al.* (2000).

Our conclusion that the Skaergaard fabrics are essentially unmodified from when they were formed at, or close to, the interface between the mush and the bulk magma is supported by the strongly foliated plagioclase-rich rocks of the UBS (Wager & Brown, 1968, fig. 93), for which the flotation of the nearly neutrally buoyant plagioclase could not exert sufficient force to be responsible for their almost adcumulate nature. Instead the strong fabric in these rocks must have been caused by grain arrangement by magmatic currents.

The lineations observed in the trough band samples (Fig. 13) are consistent with these features being channel structures (Wager & Deer, 1939; Irvine & Stoesser, 1978). That lineations developed only locally is probably a consequence of the requirement that plagioclase must form elongate or prismatic crystals (and this happens only in the upper parts of the stratigraphy) and that the current strength and particle packing must be such that lineations form rather than foliations (Yamamoto & Matsuoka, 1996).

Whereas fabrics in the Layered Series gabbros are dominated by a plagioclase SPO linked with a CPO, the lowermost sample we examined, 458242 (LZa), shows a very different fabric to the others. Such a fabric, with an almost radial orientation of plagioclase and randomly oriented olivine (Figs 4c, 6a, b and 7a, b), is typical of HZ and the lower parts of LZa, but is not present at higher stratigraphic levels. We suggest that the primocrysts on the chamber floor in these early stages had less opportunity to be aligned. Instead, it is likely that plagioclase formed open crystal networks like those described by Philpotts *et al.* (1999) and Philpotts & Dickson (2000).

HOW DO ADCUMULATES FORM?

Our forensic examination of microstructures in the Skaergaard gabbros demonstrates that the cumulates underwent almost no deformation by either dislocation or diffusion creep (dissolution–reprecipitation), and therefore that the Skaergaard adcumulates could not have formed by viscous compaction. This conclusion leaves us with two outstanding questions, which are addressed in the following two sections.

How did the Skaergaard adcumulates form?

Arguments for the increasing adcumulate character upwards through the Skaergaard stratigraphy are based on the progressive decrease in bulk-rock P_2O_5 content (e.g. Table 1, until apatite arrives as a cumulus phase in UZb), and in bulk-rock U and Rb content

through the entire stratigraphy to the Sandwich Horizon (Tegner *et al.*, 2009). If we accept this model, then we can argue that adcumulate formation may have occurred either by compositional convection in the mushy layer (Sparks *et al.*, 1985; Tait & Jaupart, 1992) or by processes resulting in the primary growth of adcumulate [as argued by Wager *et al.* (1960), Wager (1963), Wager & Brown (1968), Campbell (1978, 1987) and Morse (1986)].

Compositional convection relies on a decreasing density of the liquid during fractionation; this has been argued to be the case for the Skaergaard liquid from LZc upwards (Toplis *et al.*, 2008). However, there is strong evidence that the interstitial liquid entered the two-liquid binodal in LZc and split into a dense Fe-rich liquid and a buoyant Si-rich liquid (Holness *et al.*, 2011). Whereas the Si-rich liquid is thought to have been mobile, rising through the crystal mush and escaping into the bulk magma, the Fe-rich conjugate would have been left behind. The consequences of this behaviour for convection within the mush are not known. A further consideration is that the mushy layer in a basaltic system needs to be of the order 100 m thick to overcome the viscous forces damping convection (Tait & Jaupart, 1992). Although it is not known how thick the mushy layer was in Skaergaard, arguments based on the stratigraphic offset between the arrival of a new cumulus phase and the associated step-change in clinopyroxene–plagioclase–plagioclase dihedral angles suggest that it was of the order of 1 m at the centre of the floor in UZ times (Holness *et al.*, 2009, 2017); this is too thin to have permitted compositional convection, but of the order at which it might be possible to create primary adcumulates by the diffusive loss of unwanted components.

It is important to recognize, however, that the arguments for an increasingly adcumulate nature upwards in the Skaergaard Layered Series are based on bulk geochemistry and rely on a binary model involving cumulus crystals (or primocrysts) and an interstitial ‘trapped’ liquid. The realization that the interstitial liquid is likely to have undergone significant *in situ* fractionation, including the preferential loss of an immiscible Si-rich conjugate, brings these ideas into question. To what extent are the MZ and UZ rocks actually adcumulate, and how much dense Fe-rich liquid solidified in them? To what extent was the loss of incompatible elements affected by the preferential loss of one of the immiscible conjugates? Until we have found a way of quantifying the amount of interstitial liquid remaining in these rocks, taking into account our new understanding of the fluid dynamical behaviour of this newly recognized complexity, we cannot actually answer these questions.

Where might we expect to see adcumulates formed by compaction?

Although we do not find evidence for compaction driven by viscous deformation in Skaergaard, this does

not mean that compaction is not a viable mechanism for creating adcumulates. Compaction requires time and a driving force provided by the mass of the crystal mush. Compaction will therefore be easiest in large and/or deep (and hence slowly cooled) intrusions in which the floor mush is thick and formed of dense minerals. The densest minerals found in gabbroic systems are the Fe–Ti oxides, and therefore one might expect to see compaction by viscous deformation in intrusions containing abundant oxide primocrysts. Little is known about how the thickness of the crystal mushy layer might change systematically within intrusions, although one might expect that it will become thinner with increasing magma evolution as the temperature difference between the liquidus of the bulk magma and the solidus decreases with progressive fractionation. The thickest mushes might then be expected in magma chambers containing the least evolved magmas.

The Bushveld Intrusion, South Africa

The Bushveld Intrusion is the largest on Earth, and therefore is likely to have cooled more slowly than most other intrusions. We undertook a preliminary investigation of plagioclase-rich norites from the lowest Main Zone, as sampled by a drill core 30 km east of Rustenburg in the western Bushveld. We examined samples spaced every 30 m through ~500 m of continuous drill core, with closer spacing of samples over regions of interest. The cumulates at the base of our stratigraphic interval are almost entirely undeformed, but the plagioclase in the overlying cumulates contains abundant deformation twins, with clear evidence for lattice distortion (Fig. 14a). Grain boundaries between plagioclase are irregular and are decorated with small neoblasts of irregular shape (Fig. 14b). The transition between the undeformed and the overlying deformed rocks occurs over a few metres. The extent of deformation decreases gradually through the upper 100 m of the sampled range.

That these clear signs of deformation by dislocation creep occurred in the super-solidus, at low porosities, is demonstrated by the small pockets of late-stage interstitial quartz, which are in optical continuity over several millimetres (Fig. 14c). The quartz in these rocks is entirely undeformed, with no sign of undulose extinction, in strong contrast to the neighbouring plagioclase (Fig. 14d). This is of particular significance because quartz is generally weaker than plagioclase during dislocation creep: the deformation was clearly over by the time the final liquid solidified as interstitial quartz. These observations are entirely consistent with the crystal mushy layer deforming by dislocation creep, with deformation ceasing once the porosity had reached a few vol. %.

That this deformation either resulted in significant porosity reduction or was driven by compaction is not certain. First, the plagioclase grains have not bent by more than a few tens of degrees: if we were to unbend

those grains this does not result in a significant change in the packing efficiency. We might conclude from this that the bulk of any porosity reduction was achieved either by overgrowth or by mechanical rearrangement of essentially rigid grains. Second, the evidence for significant deformation by dislocation creep is confined to a well-defined and localized stratigraphic interval. Such localized effects are not expected for compaction, which is likely to act consistently in an intrusion in steady state with relatively constant modal proportions of primocrysts in the floor mush. The deformation may be linked to a transient change in mush thickness or it is possible that the deformation was triggered by regional events, such as wholesale subsidence of the intrusion.

The Baima Intrusion, SW China

The Baima Intrusion of SW China is notable for its abundance of Fe–Ti oxides, which form thick layers (>10 m) low in the stratigraphy, consistent with the bulk magma saturating early in these phases (Zhang *et al.*, 2012). Gabbros from this intrusion contain clear evidence for deformation by dislocation creep. The plagioclase grain size is notably bimodal: the large grains are characterized by subgrains, undulose extinction, deformation twins and bending of the entire crystal (Fig. 15a and b). Grain boundaries between the large plagioclase grains are commonly either highly irregular (Fig. 15a) or decorated with well-formed neoblcasts (Fig. 15b); there is little evidence of the preservation of low-index growth faces formed in contact with abundant melt. Internal recrystallization is evident in the large grains, with any

one thin section displaying a range in the progression of development and growth of these neoblcasts (Fig. 15c–e). Clusters of neoblcasts are unimodal in size with a well-developed granular microstructure, indicative of textural equilibrium. These signs of extensive ductile deformation via dislocation creep accompanied by recrystallization are evident only in plagioclase: the associated primocrysts of pyroxene and olivine show only rare signs of subgrains or undulose extinction, consistent with them being a relatively strong phase during deformation. That plagioclase is the weaker phase is supported by the observation that clinopyroxene forms porphyroclasts in strongly deformed oceanic gabbros (Satsukawa *et al.*, 2013). This is also suggested by the observation that plagioclase enclosed in large distributed clinopyroxene oikocrysts is generally undeformed in the Baima gabbros, consistent with it being protected from deformation by a strong pyroxene framework. That the deformation was super-solidus and not a result of some post-magmatic regional deformation is demonstrated by the abundance of disequilibrium three-grain junctions, with low dihedral angles and the replacement of neoblastic plagioclase by reactive symplectites that formed from late-stage liquids (Holness *et al.*, 2011).

The microstructures in the Bushveld and Baima intrusions are very different from those observed in the Skaergaard gabbros. They accord perfectly with those expected for viscous deformation by dislocation creep. The differences between the Bushveld and Baima samples examined here are likely to be caused by

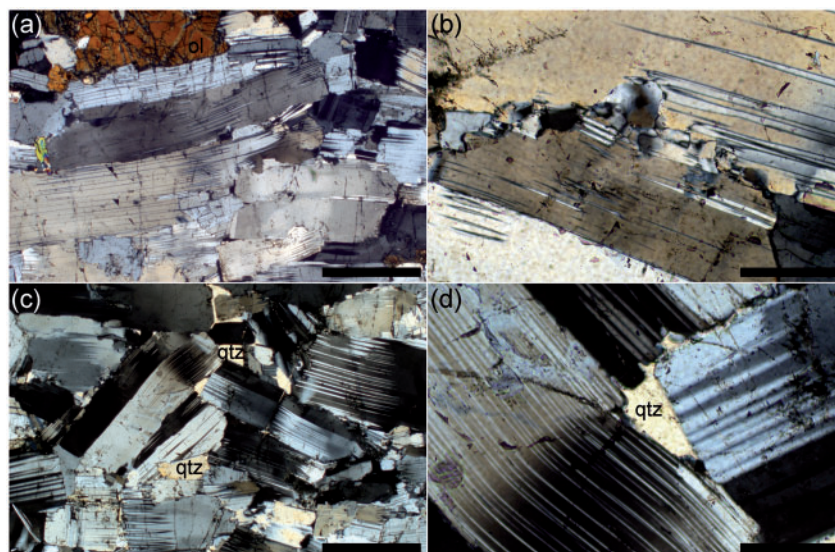


Fig. 14. Photomicrographs of microstructures in plagioclase-rich cumulates of the lower part of Main Zone, Bushveld Intrusion, South Africa. (a) Elongate plagioclase grains are bent and contain deformation twins. The irregular grain boundaries should be noted. Scale bar represents 1 mm. (b) Detail of grain boundary between two plagioclase grains, showing the development of irregular recrystallized neoblcasts during dislocation creep. Scale bar represents 200 μm . (c) Framework of deformed plagioclase grains with interstitial quartz (representative regions are labelled qtz). It should be noted that many of the quartz patches are in optical continuity, suggestive of crystallographic continuity in three dimensions. Scale bar represents 1 mm. (d) The interstitial quartz is undeformed, despite the abundant evidence for deformation during dislocation creep in the surrounding plagioclase. Quartz is significantly weaker than plagioclase: deformation must have ceased before quartz crystallized. Scale bar represents 200 μm .

differences in the extent of deformation and in the extent of accompanying recrystallization, which themselves must be caused by differences in the timing of deformation relative to solidification, grain size and the gravitational load.

We have not yet looked at compositional zoning in these rocks and therefore have not tested the idea that deformation may also have occurred by processes involving dissolution–reprecipitation.

CONCLUSIONS AND PERSPECTIVES FOR THE FUTURE

We have argued that a careful and forensic study of microstructure is an essential first step in decoding the solidification history of igneous rocks. It is clear that viscous deformation during compaction at the base of the mush, particularly by dislocation creep, leaves a clear (and potentially quantifiable) record. It is therefore essential, when advocating compaction as a significant process acting during the solidification of igneous

intrusions, that this assertion is supported by microstructural evidence. Models and hypotheses must be based on a solid foundation of fundamental observations.

Whereas the Skaergaard gabbros show very little evidence for dislocation creep, this is present in the Bushveld and Baima intrusions, which represent extreme end-members of crustal mafic intrusions (slowest-cooled or densest mush) that could have undergone viscous compaction. Importantly, although the Baima gabbros have undergone significantly more recrystallization than the Bushveld Main Zone norites, it is still possible to discern the original grains of plagioclase and therefore to distinguish between fabrics and microstructures formed deep in the mush during compaction and those formed at or close to the interface between the mush and the bulk magma. We consider it highly unlikely that any continental crustal mafic layered intrusion smaller than Bushveld, or containing a lower proportion of dense minerals than Baima, would undergo sufficient deformation by dislocation creep during

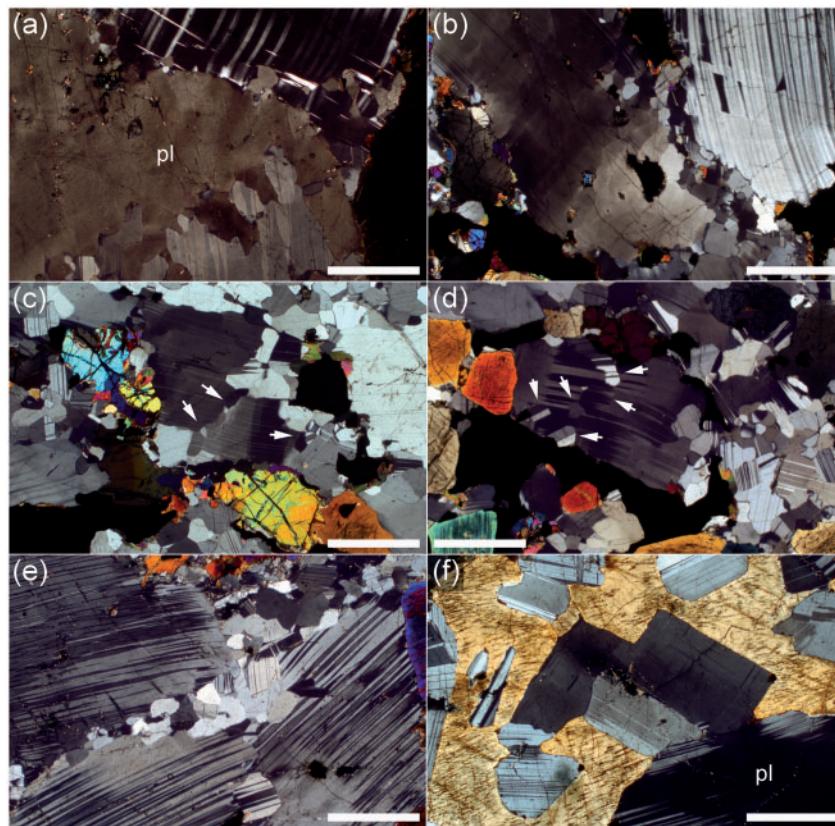


Fig. 15. Photomicrographs of plagioclase-rich cumulates from the lower part of the Baima Intrusion, SW China. All scale bars represent 1 mm. (a) Sample BM12-90, showing large plagioclase grain (labelled pl) with marked undulose extinction and a highly irregular boundary with the adjacent plagioclase grain at the bottom right. (b) Sample BM12-90. It should be noted that the plagioclase grain on the left has undulose extinction whereas that on the right has bent twins. Their mutual boundary is decorated with recrystallized neoblasts (c) Sample BM12-63. The large plagioclase grain in the centre of the field of view is bent, with the sub-grain boundary decorated with neoblasts (arrowed). (d) Sample BM12-63. The large plagioclase grain in the centre of the field of view is divided by a sub-grain boundary decorated with large neoblasts (arrowed). (e) Sample BM12-217. The grain boundaries between the three large plagioclase grains are decorated with abundant small neoblasts. (f) Sample BM12-53. The plagioclase enclosed by the clinopyroxene oikocryst is apparently undeformed, whereas the apparently unprotected grain (labelled pl) contains deformation twins.

compaction alone to result in complete recrystallization and the transposition of a magmatic fabric.

The record of diffusive deformation processes is not so easy to identify, requiring detailed examination of compositional zoning and grain shape. It is clear that the fabrics in Skaergaard were not created during diffusion-assisted creep. However, because it is unlikely that fabrics in cumulates in other intrusions would be completely overprinted by such a process, it should be possible to identify suites of related cumulates in which diffusion-assisted deformation has occurred to variable extents and therefore pinpoint its effects. It is also possible that the diffusion-assisted granular flow mechanism suggested by Paterson (2001) might be a significant process in solidifying igneous intrusions, but this hypothesis needs to be substantiated by experimental results and observation of natural examples.

Future work should be concentrated on the amalgamation of microstructural and geochemical analysis, to ascertain how adcumulates form in intrusions in which there is no evidence of the viscous deformation required for compaction, and to constrain the magnitude and timing of any effects of compaction where such evidence is present. We have mainly concentrated on plagioclase, but our work on mafic systems should be expanded in scope to look at dunitic cumulates, norites and pyroxenites. Work should also be extended to consider silicic systems, for which compaction is commonly cited as a mechanism for extracting rhyolitic liquids from a crystal-rich mush zone (e.g. Bachmann & Bergantz, 2004).

ACKNOWLEDGEMENTS

Christine Wang provided us with samples from the Baima Intrusion, and the samples from Bushveld were collected with Grant Cawthorn, with permission from Lonmin plc. We are grateful for technical support provided by Iris Buisman and Giulio Lampronti from the Earth Science Department, by Richard Langford, Eric Tapley and Jon Rickard from the Cavendish Laboratory, Cambridge University, and by Carmel Pinnington of the Earth Science EBSD-SEM Laboratory, University of Liverpool. The QEMSCAN images of the trough bands were collected during a final year undergraduate project by Katherine Monks (supervised by M.B.H. and Z.V.).

FUNDING

This work was supported by the Natural Environment Research Council [grant numbers NE/J021520/1 and NE/M000060/1] and a Royal Society International Joint Project grant. Z.V. is supported by a Marie Skłodowska-Curie Individual European Fellow grant.

SUPPLEMENTARY DATA

Supplementary data for this paper are available at *Journal of Petrology* online.

REFERENCES

- Arvidson, R. S., Beig, M. S. & Lutge, A. (2004). Single-crystal plagioclase feldspar dissolution rates measured by vertical scanning interferometry. *American Mineralogist* **89**, 51–56.
- Arzi, A. (1978). Critical phenomena in the rheology of partially melted rocks. *Tectonophysics* **44**, 173–184.
- Ashworth, J. (1980). Deformation mechanisms in mildly shocked chondritic diopside. *Meteoritics* **15**, 105–115.
- Ashworth, J. (1985). Transmission electron microscopy of L-group chondrites, 1. Natural shock effects. *Earth and Planetary Science Letters* **73**, 17–32.
- AvéLallemant, H. G. (1978). Experimental deformation of diopside and websterite. *Tectonophysics* **48**, 1–27.
- Bachmann, O. & Bergantz, G. W. (2004). On the origin of crystal-poor rhyolites: extracted from batholithic crystal mushes. *Journal of Petrology* **45**, 1565–1582.
- Bautier, M., Van Roermund, H., Drury, M. & Lardeaux, J. T. (1991). Deformation and recrystallization mechanisms in naturally deformed omphacites from the Sesia-Lanzo zone; geophysical consequences. *Tectonophysics* **195**, 11–27.
- Bédard, J. H. (2015). Ophiolitic magma chamber processes, a perspective from the Canadian Appalachians. In: Charlier, B., Namur, O., Latypov, R. & Tegner, C. (eds) *Layered Intrusions*. Berlin: Springer, pp. 693–732.
- Benn, K. & Allard, B. (1989). Preferred mineral orientations related to magmatic flow in ophiolite layered gabbros. *Journal of Petrology* **30**, 925–946.
- Bons, P. D. & den Brok, B. (2000). Crystallographic preferred orientation development by dissolution–precipitation creep. *Journal of Structural Geology* **22**, 1713–1722.
- Boorman, S., Boudreau, A. & Kruger, F. J. (2004). The Lower Zone–Critical Zone transition of the Bushveld Complex: a quantitative textural study. *Journal of Petrology* **45**, 1209–1235.
- Boudreau, A. E. & McBirney, A. R. (1997). The Skaergaard layered series. Part III. Non-dynamic layering. *Journal of Petrology* **38**, 1003–1020.
- Britton, T. B., Jiang, J., Guo, Y., Vilalta-Clemente, A., Wallis, D., Hansen, L. N., Winkelmann, A. & Wilkinson, A. J. (2016). Tutorial: crystal orientations and EBSD—or which way is up? *Materials Characterization* **117**, 113–126.
- Brothers, R. (1964). Petrofabric analyses of Rhum and Skaergaard layered rocks. *Journal of Petrology* **5**, 255–274.
- Brown, G. M. (1956). The layered ultrabasic rocks of Rhum, Inner Hebrides. *Philosophical Transactions of the Royal Society of London, Series B* **240**, 1–53.
- Campbell, I. (1978). Some problems with the cumulus theory. *Lithos* **11**, 311–323.
- Campbell, I. H. (1987). Distribution of orthocumulate textures in the Jimberlana Intrusion. *Journal of Geology* **95**, 35–54.
- Carter, N. L. & AvéLallemant, H. G. (1970). High temperature flow of dunite and peridotite. *Geological Society of America Bulletin* **81**, 2181–2202.
- Cashman, K. V., Sparks, R. S. J. & Blundy, J. D. (2017). Vertically extensive and unstable magmatic systems: a unified view of igneous processes. *Science* **355**, 1280.
- Cooper, M. R. & Hunter, R. H. (1995). Precision serial lapping, imaging and three-dimensional reconstruction of minus-cement and post-cementation intergranular pore-systems in the Penrith Sandstone of north-western England. *Mineralogical Magazine* **59**, 213–220.
- Cooper, R. F. & Kohlstedt, D. L. (1986). Rheology and structure of olivine–basalt partial melts. *Journal of Geophysical Research* **91**, 9315–9323.
- Davies, I. C. & Walker, R. G. (1974). Transport and deposition of re-sedimented conglomerates: the Cap Enrage formation, Cambro-Ordovician, Gaspé, Quebec. *Journal of Sedimentary Research* **44**, 1200–1216.

- Doherty, R. D., Hughes, D. A., Humphreys, F. J., Jonas, J. J., Juul Jensen, D., Kassner, M. E., King, W. E., McNelley, T. R., McQueen, H. J. & Rollett, A. D. (1997). Current issues in recrystallization: a review. *Materials Science and Engineering A* **238**, 219–274.
- Emeleus, C., Cheadle, M., Hunter, R., Upton, B. & Wadsworth, W. (1996). The Rum layered suite. *Developments in Petrology* **15**, 403–439.
- Fenn, P. M. (1977). The nucleation and growth of alkali feldspars from hydrous melts. *Canadian Mineralogist* **15**, 135–161.
- Fowler, A. (1990a). A compaction model for melt transport in the Earth's asthenosphere. Part I: the basic model. In: Ryan, M. P. (ed.) *Magma Transport and Storage*. Chichester: John Wiley, pp. 4–15.
- Fowler, A. (1990b). A compaction model for melt transport in the Earth's asthenosphere, part II, Applications. In: Ryan, M. P. (ed.) *Magma Transport and Storage*. Chichester: John Wiley, pp. 15–32.
- Gay, P. & Muir, I. D. (1962). Investigation of the feldspars of the Skaergaard intrusion, Eastern Greenland. *Journal of Geology* **70**, 565–581.
- German, R. M., Suri, P. & Park, S. J. (2009). Review: liquid phase sintering. *Journal of Materials Science* **44**, 1–39.
- Godard, G. & van Roermund, H. L. M. (1995). Deformation-induced clinopyroxene fabrics form eclogites. *Journal of Structural Geology* **17**, 1425–1443.
- Gray, N. H., Philpotts, A. R. & Dickson, L. D. (2003). Quantitative measures of textural anisotropy resulting from magmatic compaction illustrated by a sample from the Palisades sill, New Jersey. *Journal of Volcanology and Geothermal Research* **121**, 293–312.
- Grout, F. F. (1918). Internal structures of igneous rocks; their significance and origin; with special reference to the Duluth Gabbro. *Journal of Geology* **26**, 439–458.
- Heidelbach, F., Post, A. & Tullis, J. (2000). Crystallographic preferred orientation in albite samples deformed experimentally by dislocation and solution precipitation creep. *Journal of Structural Geology* **22**, 1649–1661.
- Higgins, M. D. (1991). The origin of laminated and massive anorthosite, Sept Iles layered intrusion, Quebec, Canada. *Contributions to Mineralogy and Petrology* **106**, 340–354.
- Holness, M. B. (2014). The effect of crystallization time on plagioclase grain shape in dolerites. *Contributions to Mineralogy and Petrology* **168**, 1–19.
- Holness, M. B. (2015). Plagioclase growth rates control three-grain junction geometry in dolerites and gabbros. *Journal of Petrology* **56**, 2117–2144.
- Holness, M. B. & Humphreys, M. C. S. (2003). The Traigh Bhàn na Sgùrra Sill, Isle of Mull: Flow localization in a major magma conduit. *Journal of Petrology* **44**, 1961–1976.
- Holness, M. B., Tegner, C., Nielsen, T. F., Stripp, G. & Morse, S. A. (2007). A textural record of solidification and cooling in the Skaergaard intrusion, East Greenland. *Journal of Petrology* **48**, 2359–2377.
- Holness, M. B., Tegner, C. & Nielsen, T. F. (2009). Constraining the thickness of the crystal mush in layered mafic intrusions. American Geophysical Union, Fall Meeting 2009, abstract V13F-05.
- Holness, M. B., Stripp, G., Humphreys, M. C. S., Veklsler, I. V., Nielsen, T. F. D. & Tegner, C. (2011). Silicate liquid immiscibility within the crystal mush: late-stage magmatic microstructures in the Skaergaard Intrusion, East Greenland. *Journal of Petrology* **52**, 175–222.
- Holness, M. B., Humphreys, M., Sides, R., Helz, R. T. & Tegner, C. (2012a). Toward an understanding of disequilibrium dihedral angles in mafic rocks. *Journal of Geophysical Research: Solid Earth* **117**, B06207, doi:10.1029/2011JB008902.
- Holness, M. B., Sides, R., Prior, D. J., Cheadle, M. J. & Upton, B. G. (2012b). The peridotite plugs of Rum: Crystal settling and fabric development in magma conduits. *Lithos* **134**, 23–40.
- Holness, M. B., Tegner, C., Namur, O. & Pilbeam, L. (2015). The earliest history of the Skaergaard magma chamber: a textural and geochemical study of the Cambridge drill core. *Journal of Petrology* **56**, 1199–1227.
- Holness, M. B., Tegner, C., Nielsen, T. F. D. & Charlier, B. (2017). The thickness of the mushy layer on the floor of the Skaergaard magma chamber at apatite saturation. *Journal of Petrology*, doi:10.1093/petrology/egx040.
- Holtzman, B. K., Groebner, N. J., Zimmerman, M. E., Ginsberg, S. B. & Kohlstedt, D. L. (2003). Deformation-driven melt segregation in partially molten rocks. *Geochemistry, Geophysics, Geosystems* **4**, 8607.
- Hoover, J. D. (1989). Petrology of the Marginal Border Series of the Skaergaard intrusion. *Journal of Petrology* **30**, 399–439.
- Housden, J., O'Reilly, W. & Day, S. (1995). Variations in magnetic properties of Unit 10, Eastern Layered Intrusion, Isle of Rum, Scotland: implications for patterns of high temperature hydrothermal alteration. *Transactions of the Royal Society of Edinburgh: Earth Science* **86**, 91–112.
- Hoyer, L. & Watkeys, M. K. (2015). Assessing SPO techniques to constrain magma flow: Examples from sills of the Karoo Igneous Province, South Africa. *Tectonophysics* **656**, 61–73.
- Humphreys, M. C. S. (2009). Chemical evolution of intercumulus liquid, as recorded in plagioclase overgrowth rims from the Skaergaard Intrusion. *Journal of Petrology* **50**, 127–145.
- Humphreys, M. C. (2011). Silicate liquid immiscibility within the crystal mush: evidence from Ti in plagioclase from the Skaergaard intrusion. *Journal of Petrology* **52**, 147–174.
- Hunter, R. H. (1996). Textural development in cumulate rocks. In: Cawthorn, G. A. (ed.) *Layered Intrusions*. Amsterdam: Elsevier, pp. 77–101.
- Ildefonse, B. (1987). Les lineations et la déformation: aspects naturels, théoriques et expérimentaux des orientations préférentielles de forme. PhD thesis, Université de Lyon.
- Ingrin, J., Doukhan, N. & Doukhan, J. (1991). High-temperature deformation of diopside single crystals: 2. Transmission electron microscopy investigation of the defect microstructures. *Journal of Geophysical Research: Solid Earth* **96**, 14287–14297.
- Irvine, T. N. (1980). Magmatic infiltration metasomatism, double diffusive fractional crystallisation and adcumulus growth in the Muskox Intrusion and other layered intrusions. In: Hargraves, R. B. (ed.) *Physics of Magmatic Processes*. Princeton, NJ: Princeton University Press, pp. 325–383.
- Irvine, T. (1983). Skaergaard trough-layering structures. *Carnegie Institution of Washington Year Book* **82**, 289–295.
- Irvine, T. & Stoesser, D. (1978). Structure of the Skaergaard trough bands. *Annual Reports of the Director of the Geophysical Laboratory, Carnegie Institution of Washington Year Book* **77**, 725–732.
- Irvine, T. N., Andersen, J. C. Ø. & Brooks, C. K. (1998). Included blocks (and blocks within blocks) in the Skaergaard intrusion: Geologic relations and the origins of rhythmic modally graded layers. *Geological Society of America Bulletin* **110**, 1398–1447.
- Iso, Y., Cohen, C. & Koch, D. L. (1996). Orientation in simple shear flow of semi-dilute fiber suspensions 2. Highly elastic fluids. *Journal of Non-Newtonian Fluid Mechanics* **62**, 135–153.
- Jakobsen, J. K., Tegner, C., Brooks, C. K., Kent, A. J., Leshner, C. E., Nielsen, T. F. & Wiedenbeck, M. (2010). Parental magma of the Skaergaard intrusion: constraints from melt inclusions in primitive troctolite blocks and FG-1 dykes. *Contributions to Mineralogy and Petrology* **159**, 61–79.

- Ji, S. & Mainprice, D. (1990). Recrystallization and fabric development in plagioclase. *Journal of Geology* **98**, 65–79.
- Ji, S., Mainprice, D. & Boudier, F. (1988). Sense of shear in high-temperature movement zones from the fabric asymmetry of plagioclase feldspars. *Journal of Structural Geology* **10**, 73–81.
- Jung, H. & Karato, S. I. (2001). Water-induced fabric transitions in olivine. *Science* **293**, 1460–1463.
- Karato, S. I. (1988). The role of recrystallization in the preferred orientation of olivine. *Physics of the Earth and Planetary Interiors* **51**, 107–122.
- Katayama, I., Jung, H. & Karato, S. I. (2004). New type of olivine fabric from deformation experiments at modest water content and low stress. *Geology* **32**, 1045–1048.
- King, D. S., Zimmerman, M. E. & Kohlstedt, D. L. (2009). Stress-driven melt segregation in partially molten olivine-rich rocks deformed in torsion. *Journal of Petrology* **51**, 21–42.
- Kirkpatrick, R. J. (1974). Kinetics of crystal growth in the system $\text{CaMgSi}_2\text{O}_6\text{--CaAl}_2\text{SiO}_6$. *American Journal of Science* **274**, 215–242.
- Klein, L. & Ullmann, D. R. (1974). Crystallisation behaviour of anorthite. *Journal of Geophysical Research* **79**, 4869–4874.
- Mainprice, D. & Nicolas, A. (1989). Development of shape and lattice preferred orientations: application to the seismic anisotropy of the lower crust. *Journal of Structural Geology* **11**, 175–189.
- Mauler, A., Bystricky, M., Kunze, K. & Mackwell, S. (2000). Microstructures and lattice preferred orientations in experimentally deformed clinopyroxene aggregates. *Journal of Structural Geology* **22**, 1633–1648.
- McBirney, A. R. (1975). Differentiation of the Skaergaard Intrusion. *Nature* **253**, 691–694.
- McBirney, A. R. (1989a). The Skaergaard Layered Series: I. Structure and average compositions. *Journal of Petrology* **30**, 363–397.
- McBirney, A. R. (1989b). Geological map of the Skaergaard Intrusion, East Greenland, 1:20 000. Eugene, OR: Department of Geology, University of Oregon.
- McBirney, A. R. & Nicolas, A. (1997). The Skaergaard layered series. Part II. Magmatic flow and dynamic layering. *Journal of Petrology* **38**, 569–580.
- McClay, K. R. (1977). Pressure solution and Coble creep in rocks and minerals: a review. *Journal of the Geological Society, London* **134**, 57–70.
- McKenzie, D. (1984). The generation and compaction of partially molten rock. *Journal of Petrology* **25**, 713–765.
- McKenzie, D. (1985). The extraction of magma from the crust and mantle. *Earth and Planetary Science Letters* **74**, 81–91.
- McKenzie, D. (2011). Compaction and crystallization in magma chambers: towards a model of the Skaergaard Intrusion. *Journal of Petrology* **52**, 905–930.
- Mecklenburgh, J., Zhao, Y. H., Heidelbach, F. & Mackwell, S. (2006). Deformation of olivine–spinel aggregates in the system $(\text{Mg,Ni})_2\text{GeO}_4$ deformed to high strain in torsion: implications for upper mantle anisotropy. *Journal of Geophysical Research: Solid Earth* **111**, B11209, doi:10.1029/2006JB004285.
- Mehl, L. & Hirth, G. (2008). Plagioclase preferred orientation in layered mylonites: evaluation of flow laws for the lower crust. *Journal of Geophysical Research: Solid Earth* **113**, B05202, doi:10.1029/2007JB005075.
- Meurer, W. & Boudreau, A. (1998). Compaction of igneous cumulates part II: compaction and the development of igneous foliations. *Journal of Geology* **106**, 293–304.
- Meurer, W. & Meurer, M. (2006). Using apatite to dispel the ‘trapped liquid’ concept and to understand the loss of interstitial liquid by compaction in mafic cumulates: an example from the Stillwater Complex, Montana. *Contributions to Mineralogy and Petrology* **151**, 187–201.
- Miyazaki, T., Sueyoshi, K. & Hiraga, T. (2013). Olivine crystals align during diffusion creep of Earth’s upper mantle. *Nature* **502**, 321–326.
- Montardi, Y. & Mainprice, D. (1987). A transmission electron microscopic study of the natural plastic deformation of calcic plagioclases ($\text{An}_{68 \pm 70}$). *Bulletin Minéralogique* **110**, 1–14.
- Morales, L. F., Boudier, F. & Nicolas, A. (2011). Microstructures and crystallographic preferred orientation of anorthosites from Oman ophiolite and the dynamics of melt lenses. *Tectonics* **30**, TC2011, doi:10.1029/2010TC002697.
- Morse, S. (1986). Convection in aid of acumulus growth. *Journal of Petrology* **27**, 1183–1214.
- Namur, O., Humphreys, M. C. S. & Holness, M. B. (2014). Crystallization of interstitial liquid and latent heat buffering in solidifying gabbros: Skaergaard intrusion, Greenland. *Journal of Petrology* **55**, 1389–1427.
- Naslund, H. (1984). Supersaturation and crystal growth in the roof-zone of the Skaergaard magma chamber. *Contributions to Mineralogy and Petrology* **86**, 89–93.
- Nicolas, A. (1992). Kinematics in magmatic rocks with special reference to gabbros. *Journal of Petrology* **33**, 891–915.
- Nielsen, T. F. (2004). The shape and volume of the Skaergaard intrusion, Greenland: implications for mass balance and bulk composition. *Journal of Petrology* **45**, 507–530.
- Nielsen, T. F. D., Andersen, J. C. Ø., Holness, M. B., Keiding, J. K., Rudashevsky, N. S., Rudashevsky, V. N., Salmonsén, L. P., Tegner, C. & Veksler, I. V. (2015). The Skaergaard PGE and gold deposit: the result of *in situ* sulphide saturation and magma chamber-scale precious metal redistribution by immiscible Fe-rich melt. *Journal of Petrology* **56**, 1643–1676.
- Nwe, Y. Y. (1975). Aspects of the mineralogy of the Skaergaard intrusion, East Greenland. PhD thesis, University of Cambridge.
- O’Driscoll, B., Hargraves, R., Emeleus, C., Troll, V., Donaldson, C. & Reavy, R. (2007). Magmatic lineations inferred from anisotropy of magnetic susceptibility fabrics in Units 8, 9, and 10 of the Rum Eastern Layered Series, NW Scotland. *Lithos* **98**, 27–44.
- O’Driscoll, B., Stevenson, C. T. & Troll, V. R. (2008). Mineral lamination development in layered gabbros of the British Palaeogene Igneous Province: A combined anisotropy of magnetic susceptibility, quantitative textural and mineral chemistry study. *Journal of Petrology* **49**, 1187–1221.
- Olesen, N. Ø. (1987). Plagioclase fabric development in a high-grade shear zone, Jotunheimen, Norway. *Tectonophysics* **142**, 291–308.
- Olsen, T. S. & Kohlstedt, D. L. (1984). Analysis of dislocations in some naturally deformed plagioclase feldspars. *Physics and Chemistry of Minerals* **11**, 153–160.
- Paterson, M. S. (1995). A theory for granular flow accommodated by material transfer via an intergranular fluid. *Tectonophysics* **245**, 135–151.
- Paterson, M. S. (2001). A granular flow theory for the deformation of partially molten rock. *Tectonophysics* **335**, 51–61.
- Paterson, S. R., Fowler, T. K., Jr, Schmidt, K. L., Yoshinobu, A. S., Yuan, E. S. & Miller, R. B. (1998). Interpreting magmatic fabric patterns in plutons. *Lithos* **44**, 53–82.
- Philippot, P. & van Roermund, H. L. (1992). Deformation processes in eclogitic rocks: evidence for the rheological delamination of the oceanic crust in deeper levels of subduction zones. *Journal of Structural Geology* **14**, 1059–1077.
- Philpotts, A. R. & Dickson, L. D. (2000). The formation of plagioclase chains during convective transfer in basaltic magma. *Nature* **406**, 59–61.

- Philpotts, A. R. & Philpotts, D. E. (2005). Crystal-mush compaction in the Cohasset flood-basalt flow, Hanford, Washington. *Journal of Volcanology and Geothermal Research* **145**, 192–206.
- Philpotts, A. R., Carroll, M. R. & Hill, J. M. (1996). Crystal-mush compaction and the origin of pegmatitic segregation sheets in a thick flood-basalt flow in the Mesozoic Hartford Basin, Connecticut. *Journal of Petrology* **37**, 811–836.
- Philpotts, A. R., Brustman, C. M., Shi, J., Carlson, W. D. & Denison, C. (1999). Plagioclase-chain networks in slowly cooled basaltic magma. *American Mineralogist* **84**, 1819–1829.
- Picard, D., Arbaret, L., Pichavant, M., Champallier, R. & Launeau, P. (2013). The rheological transition in plagioclase-bearing magmas. *Journal of Geophysical Research: Solid Earth* **118**, 1363–1377.
- Prior, D. J., Mariani, E. & Wheeler, J. (2009). EBSD in the earth sciences: Applications, common practice, and challenges. In: Schwartz, A. J., Kumar, M., Adams, B. L. & Field, D. P. (eds) *Electron Backscatter Diffraction in Materials Science*. New York: Springer, pp. 345–360, doi:10.1007/978-0-387-88136-2_26.
- Richter, F. M. & McKenzie, D. (1984). Dynamical models for melt segregation from a deformable matrix. *Journal of Geology* **92**, 729–740.
- Rosenberg, C. L. & Handy, M. R. (2005). Experimental deformation of partially melted granite revisited: implications for the continental crust. *Journal of Metamorphic Geology* **23**, 19–28.
- Rust, B. R. (1972). Pebble orientation in fluvial sediments. *Journal of Sedimentary Research* **42**, 384–388.
- Rutter, E. H. (1983). Pressure solution in nature, theory and experiment. *Journal of the Geological Society, London* **140**, 725–740.
- Rutter, E. (1997). The influence of deformation on the extraction of crustal melts: a consideration of the role of melt-assisted granular flow. In: Holness, M. B. (ed.) *Deformation-enhanced Fluid Transport in the Earth's Crust and Mantle. Mineralogical Society Series* **8**, 82–110.
- Rutter, E. & Neumann, D. H. K. (1995). Experimental deformation of partially molten Westerley granite under fluid-absent conditions, with implications for the extraction of granitic magmas. *Journal of Geophysical Research* **100**, 15697–15715.
- Rutter, E., Casey, M. & Burlini, L. (1994). Preferred crystallographic orientation development during the plastic and superplastic flow of calcite rocks. *Journal of Structural Geology* **16**, 1431–1446.
- Salmonsén, L. P. & Tegner, C. (2013). Crystallization sequence of the Upper Border Series of the Skaergaard Intrusion: revised subdivision and implications for chamber-scale magma homogeneity. *Contributions to Mineralogy and Petrology* **165**, 1155–1171.
- Satsukawa, T., Ildefonse, B., Mainprice, D., Morales, L., Michibayashi, K. & Barou, F. (2013). A database of plagioclase crystal preferred orientations (CPO) and microstructures—implications for CPO origin, strength, symmetry and seismic anisotropy in gabbroic rocks. *Solid Earth* **4**, 511.
- Schmidt, M. W., Forien, M., Solferino, G. & Bagdassarov, N. (2012). Settling and compaction of olivine in basaltic magmas: an experimental study on the time scales of cumulate formation. *Contributions to Mineralogy and Petrology* **164**, 959–976.
- Scott, D. R. & Stevenson, D. J. (1984). Magma solitons. *Geophysical Research Letters* **11**, 1161–1164.
- Scott, D. R. & Stevenson, D. J. (1986). Magma ascent by porous flow. *Journal of Geophysical Research: Solid Earth* **91**, 9283–9296.
- Shelley, D. (1985). Determining paleo-flow directions from groundmass fabrics in the Lyttelton radial dykes, New Zealand. *Journal of Volcanology and Geothermal Research* **25**, 69–79.
- Shelley, D. (1986). Natural deformation and recrystallisation of some intermediate plagioclase feldspars—a discussion on preferred orientation development. *Tectonophysics* **124**, 359–364.
- Shirley, D. N. (1986). Compaction of igneous cumulates. *Journal of Geology* **94**, 795–809.
- Song, C., Wang, P. & Makse, H. A. (2008). A phase diagram for jammed matter. *Nature* **453**, 629–632.
- Sparks, R. S. J., Kerr, R. C., McKenzie, D. P. & Tait, S. R. (1985). Postcumulus processes in layered intrusions. *Geological Magazine* **122**, 555–568.
- Stipp, M., Stünitz, H., Heilbronner, R. & Schmid, S. M. (2002). The eastern Tonale fault zone: a 'natural laboratory' for crystal plastic deformation of quartz over a temperature range from 250 to 700°C. *Journal of Structural Geology* **24**, 1861–1884.
- Svahnberg, H. & Piazzolo, S. (2013). Interaction of chemical and physical processes during deformation at fluid-present conditions: a case study from an anorthosite-leucogabbro deformed at amphibolite facies conditions. *Contributions to Mineralogy and Petrology* **165**, 543–562.
- Swanson, S. E. (1977). Relation of nucleation and crystal-growth rate to the development of granitic textures. *American Mineralogist* **62**, 966–978.
- Tait, S. & Jaupart, C. (1992). Compositional convection in a reactive crystalline mush and melt differentiation. *Journal of Geophysical Research: Solid Earth* **97**, 6735–6756.
- Tegner, C., Thy, P., Holness, M. B., Jakobsen, J. K. & Leshner, C. E. (2009). Differentiation and compaction in the Skaergaard Intrusion. *Journal of Petrology* **50**, 813–840.
- Tepley, F. J. & Davidson, J. P. (2003). Mineral-scale Sr-isotope constraints on magma evolution and chamber dynamics in the Rum layered intrusion, Scotland. *Contributions to Mineralogy and Petrology* **145**, 628–641.
- Tharp, T. M., Loucks, R. R. & Sack, R. O. (1998). Modeling compaction of olivine cumulates in the Muskox intrusion. *American Journal of Science* **298**, 758–790.
- Toplis, M. J., Brown, W. L. & Pupier, E. (2008). Plagioclase in the Skaergaard intrusion. Part 1: Core and rim compositions in the Layered Series. *Contributions to Mineralogy and Petrology* **155**, 329–340.
- Tullis, J. (1975). Deformation of feldspars. In: Ribbe, P. H. (ed.) *Feldspar Mineralogy. Mineralogical Society of America, Reviews in Mineralogy* **2**, 297–323.
- Van der Molen, I. & Paterson, M. (1979). Experimental deformation of partially-melted granite. *Contributions to Mineralogy and Petrology* **70**, 299–318.
- Van Roermund, H. L. (1984). Omphacite microstructures. *Textures and Microstructures* **6**, 105–116.
- Van Roermund, H. & Boland, J. (1981). The dislocation substructures of naturally deformed omphacites. *Tectonophysics* **78**, 403–418.
- VanTongeren, J. A., Hirth, G. & Kelemen, P. B. (2015). Constraints on the accretion of the gabbroic lower oceanic crust from plagioclase lattice preferred orientation in the Samail ophiolite. *Earth and Planetary Science Letters* **427**, 249–261.
- Vernon, R. H. (2004). *A Practical Guide to Rock Microstructure*. Cambridge: Cambridge University Press, 594 pp.
- Vigneresse, J. L. & Tikoff, B. (1999). Strain partitioning during partial melting and crystallising felsic magmas. *Tectonophysics* **312**, 117–132.

- Wager, L. (1963). The mechanism of adcumulus growth in the layered series of the Skaergaard intrusion. In: *Mineralogical Society of America, Special Paper 1*, 1–9.
- Wager, L. R. & Brown, G. M. (1968). *Layered Igneous Rocks*. Edinburgh: Oliver & Boyd.
- Wager, L. R. & Deer, W. A. (1939). Geological investigations in East Greenland. Part III. The petrology of the Skaergaard intrusion, Kangerdlussuaq, East Greenland. *Meddelelser om Grønland* **105**(4).
- Wager, L. R., Brown, G. M. & Wadsworth, W. J. (1960). Types of igneous cumulates. *Journal of Petrology* **1**, 73–85.
- Worrell, L. R. (2002). The origin of igneous cumulates: integrated studies of peridotites from the Western Layered Series of the Rum Layered Intrusion. PhD thesis, University of Liverpool.
- Yamamoto, S. & Matsuoka, T. (1996). Dynamic simulation of microstructure and rheology of fiber suspensions. *Polymer Engineering and Science* **36**, 2396–2403.
- Zhang, X.-Q., Song, X.-Y., Chen, L.-M., Xie, W., Yu, S.-Y., Zheng, W.-Q., Deng, Y.-F., Zhang, J.-F. & Gui, S.-G. (2012). Fractional crystallization and the formation of thick Fe–Ti–V oxide layers in the Baima layered intrusion, SW China. *Ore Geology Reviews* **49**, 96–108.

